Journal of Sedimentary Research

Journal of Sedimentary Research, 2011, v. 81, 185–206
Research Article
DOI: 10.2110/jsr.2011.21

ANALYZING SPATIAL PATTERNS IN MODERN CARBONATE SAND BODIES FROM GREAT BAHAMA BANK

PAUL M. (MITCH) HARRIS,[1] SAMUEL J. PURKIS,[2] AND JAMES ELLIS[3]
[1]*Chevron Energy Technology Company, San Ramon, California, U.S.A.*
[2]*National Coral Reef Institute, Nova Southeastern University, Dania Beach, Florida, U.S.A.*
[3]*Ellis GeoSpatial, Walnut Creek, California, U.S.A.*
e-mail: mitchharris@chevron.com

ABSTRACT: **Three carbonate sand bodies on Great Bahama Bank, which show a range of depositional facies patterns typifying modern deposits as well as their ancient counterparts, are quantitatively interrogated to broaden our perspective of the types of information that can be derived from studies of modern environments. Rimming the southern end of Tongue of the Ocean (TOTO) is the broadest expanse of "high-energy" sands found in the Bahamas, characterized by narrow sandbars separated by wide, deep channels and a lack of islands. A variation of the tidal-bar motif with broader and more irregular sandbars, relatively narrow channels, and few small islands occurs at the northern end of Exuma Sound (Schooners). Sands associated with tidal channels and the numerous islands of the Exumas chain along the western edge of Exuma Sound occur primarily as flood tidal deltas.**

The geometry of sandbars that inhabit the three sand bodies is quantified using Landsat remote sensing and assembled, along with optically derived bathymetric surfaces, into a GIS. This database is quantitatively examined using a suite of morphometric tools to compare and contrast geometric character of sandbars within and between the three sand bodies. Considered are properties such as the size, shape, complexity, distribution, orientation, and topography of the individual sandbars. Profiles and spatial analysis tools enable sandbar and channel spacing, position relative to the platform margin, connectedness, separation distances, and density to be characterized. As has been previously reported for reef-dominated environments, certain aspects of the geometry of the three systems are found to behave in a systematic and hence predictable manner, though important mathematical differences are revealed between the scaling of reefal landscapes and the grainy geobodies considered by this study. Because the three sand bodies are disparate in their overall extent and depositional settings (e.g., orientation, prevalence of islands), this predictable behavior has the potential to impart considerable insight to the characterization of grainstone systems.

INTRODUCTION

Remote sensing data and GIS of three prominent sand bodies from Great Bahama Bank (GBB) are used to map and analyze modern shallow-water deposits with a goal of deciphering quantitative relationships and thereby broadening our perspective of the types of information that can be derived from studies of the modern. The results build upon those of Purkis et al. (2005), Purkis et al. (2007), Purkis et al. (2010), and Harris and Vlaswinkel (2008), who, in contrast to this study, which considers a grain-dominated system, analyzed the morphometric properties of reefal environments. Though the depositional setting may differ, the ultimate motivation of this work is the same as for reef-focused studies; that is, to provide quantitative approaches with the analysis of modern depositional systems. As for Purkis et al. (2007), it is envisioned that statistics of this type can be used to both drive "pattern replicating" algorithms, and/or validate "process imitating" models.

The three sand bodies on GBB that are described in this study—TOTO, Schooners, and the Exumas—generally parallel the platform edge and show a range of depositional patterns that typify these types of modern environments (Fig. 1). The three visible bands of Landsat TM and ETM+ imagery were processed to maximize water penetration and produce the visible-light color composites of Figure 2. The clear water and relatively consistent, light seafloor color support using the digital numbers of each offshore pixel in the Landsat ETM+ Band 1 (reflected blue light) as an approximation of water depth (*sensu* Harris and Kowalik 1994; Harris and Ellis 2009; Harris et al. 2010); therefore Band 1 was used to develop the bathymetric digital elevation models (DEMs) of Figure 1. The brightness and water-depth relationships are only an approximation for TOTO and Schooners because of the relative lack of depth measurements as control points, whereas the relationship is better constrained for the Exumas, where more depth soundings are available from published navigation charts (Harris and Ellis 2009; Harris et al. 2010). Even given the lack of depth soundings for training, the resulting bathymetric DEMs for all three sand bodies appear geologically reasonable when compared with field maps derived from the respective areas and our own observations in the field.

Harris and Ellis (2009) and Harris (2010) provide a set of processed satellite images and an offshore/onshore digital elevation model (DEM) for the Exumas, and show examples of geologic interpretation and morphometric interpretation from the imagery. This current study broadens their lines of investigation by comparing three different sand bodies with varying characteristics, exploring different approaches for defining sandbars within the sand bodies, and significantly increasing the quantitative analysis by employing a wider range of techniques.

The expanded digital publication of Harris et al. (2010) provides details of the workflows applied to the satellite imagery for the three sand bodies

 1527-1404/11/081-185/$03.00

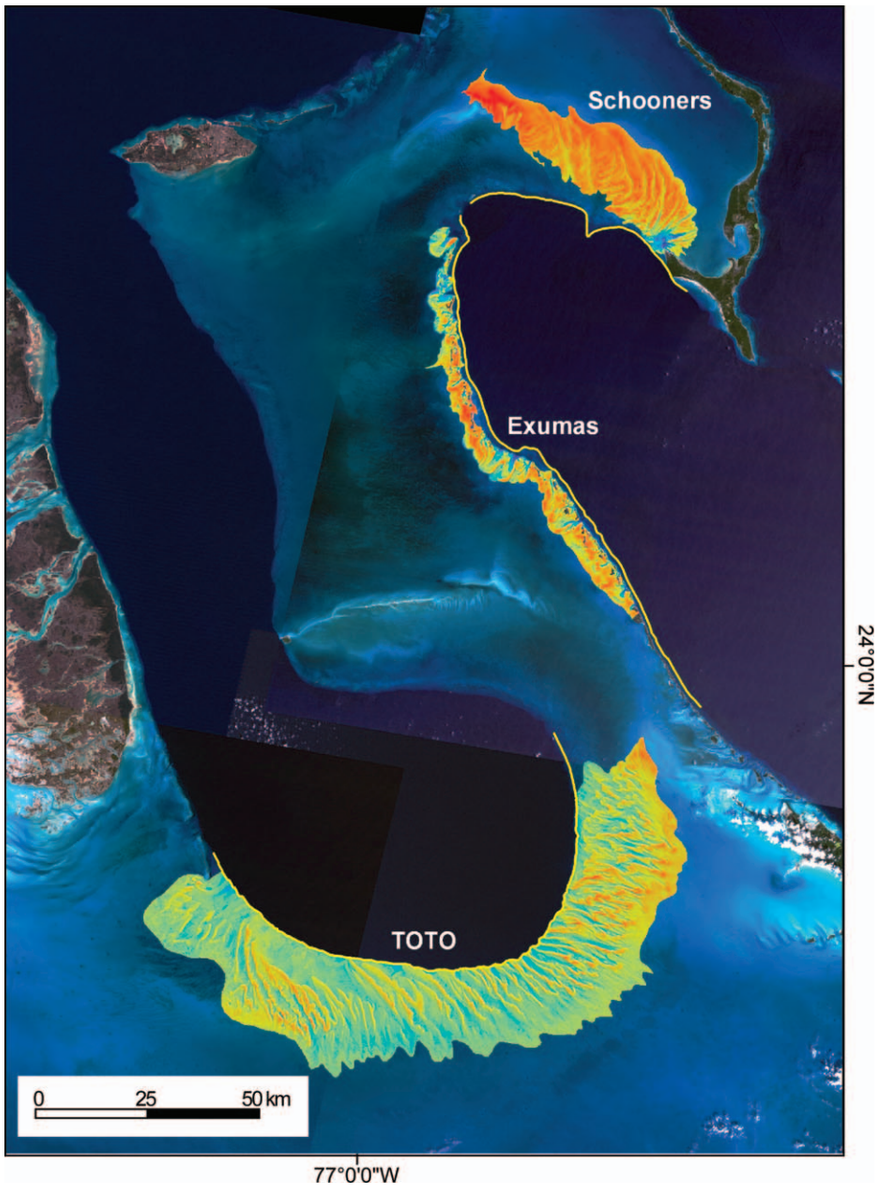

FIG. 1.—Landsat imagery identifying the three sand deposits of GBB (TOTO, Schooners, and Exumas) that are the focus of this study. The sand deposits are highlighted by showing in color their respective digital elevation models (DEMs).

discussed herein, including image processing, derivation and contouring of DEMs, and rationale for sandbar polygons, centerlines, interpretation maps, and morphometric analyses. Included in their publication is an ~ 3.2 GB database with satellite images, DEMs, and interpretation maps in GeoTiff with tfw (world file) format. To expedite display in ESRI's ArcGIS 9.3, mxd and sdx files are included that automatically load select files into ArcMap or 3D Analyst/ArcScene (perspective views). Files are also included with an objective of moving the geospatial data from the GIS into lower cost, more readily available viewers, e.g., GeoPDF, Google Earth, animation, and ArcExplorer, to support training and improve communication. Readers stimulated by the concepts presented in the following discussion are encouraged to examine Harris et al. (2010) for additional documentation of the workflows and approaches summarized herein, further examples and illustrations of the morphometric results, and an opportunity to explore and experiment with the exhaustive geospatial database.

GBB Sand Bodies

GBB displays a well-organized association of shallow, platform-top depositional environments (Purdy 1963; Traverse and Ginsburg 1966; Enos 1974; Reijmer et al. 2009). Typically, thicker accumulations of modern sediments are concentrated along the margin of the platform, which is a focus of sediment production and deposition, and included in these platform-margin deposits are ooid sand bodies (Newell et al. 1960; Purdy 1961; Ball 1967; Hine 1977; Harris 1979; Halley et al. 1983; Harris 2010; Kaczmarek et al. 2010). Ooid sand bodies are generally formed of long and narrow sandbars with varying sinuosity (tidal bar belt of Ball 1967) or lobe-shaped sandbars (marine sand belt of Ball 1967) that alternate with tidal channels and trend nearly perpendicular to the length of the sand body. Alternatively, gaps between islands laterally restrict and concentrate tidal currents and may promote development of tidal deltas (Ball 1967; Rankey et al. 2006; Reeder and Rankey 2008 2009; Harris and

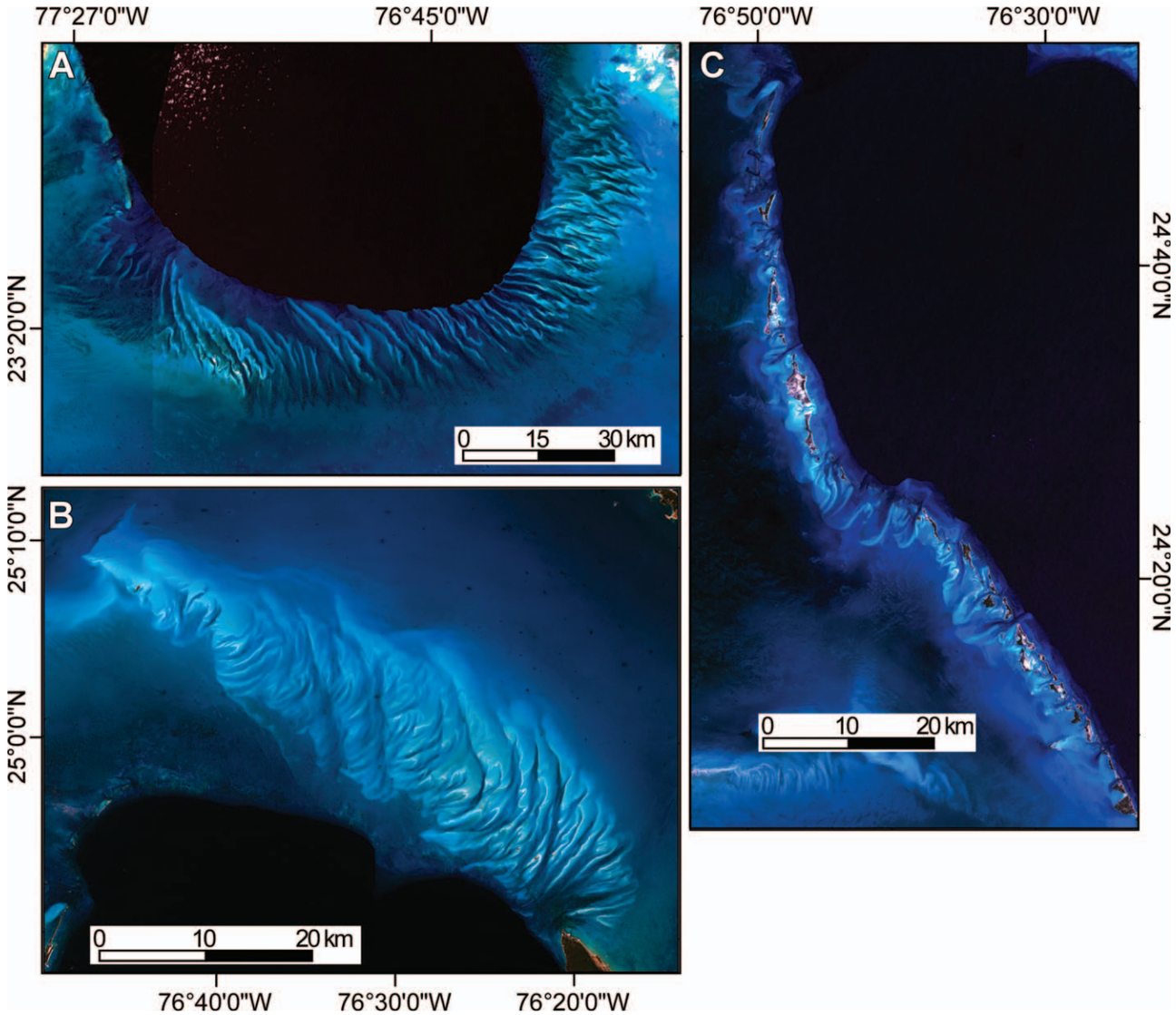

FIG. 2.—Landsat images of **A)** southern cul-de-sac portion of TOTO showing the expansive tidal bar and channel belt, **B)** the northern portion of Exuma Sound showing the tidal bar and channel belt of the Schooners, and **C)** the northwestern portion of Exuma Sound showing the tidal deltas, tidal channels, and islands of the Exumas.

Ellis 2009; Harris 2010). Tidal flow and wave-generated currents cause the sands to be in motion over much of the length of the individual sandbars or lobes, because there is a tidal exchange of water between the seaward and bankward sides of the sand body through the channels (Rankey et al. 2006; Reeder and Rankey 2008). Embayments such as TOTO and Exuma Sound on GBB are examples of a particular setting that gives rise to strong currents by amplification of tidal flow (Ball 1967).

Rimming the southern end of TOTO is the broadest expanse of "high-energy" sands found in the Bahamas (Purdy 1961; Ball 1967; Palmer 1979; Halley et al. 1983; Harris and Kowalik 1994), a tidal bar and channel belt (*sensu* Ball 1967) extending parallel to the platform edge for 155 km and covering 3120 km^2 (Fig. 2A). This sand body is generally characterized by long, narrow sandbars separated by wide, deep channels and a lack of islands. Individual sandbars extend onto the shallow platform on average 20 km but up to 27 km. The sandbars and channels gently curve and trend at a high angle to the long axis of the sand body, which itself varies considerably in direction as it wraps around the southern end of the cul-de-sac of TOTO. The character of the sandbars and channels is not uniform throughout the length of the sand body. The central portion is typified by long, linear sandbars that parallel each other and whose seaward terminations are coincident with the platform edge. Sandbars to the northeast also hug the platform edge, but individual sandbars are commonly not as long and they are typified by irregular, even parabolic shapes that trend in multiple directions. The sandbars to the west are set back from the platform edge, narrow, subparallel, and sinuous in part.

A variation of the tidal-bar motif occurs at the northern end of Exuma Sound, the Schooners (Ball 1967; Dravis 1977; Harris and Kowalik 1994; Rankey et al. 2008). Although the Schooners Cays area was used by Ball (1967) to describe the tidal-bar-belt style of sand body, which also includes TOTO, the two areas are in fact quite different. In this case, the sand body, covering 716 km^2 and extending along the platform edge for

62 km, is progressively set back from the platform edge toward the west (Fig. 2B). In comparison to TOTO, Schooners contains broader and more irregular sandbars up to 17 km long, averaging 12 km, with relatively narrow channels and few small islands. As with TOTO, the character of the sandbars and channels in the Schooners is not uniform throughout the length of the sand body. The southeastern portion of Schooners, which is perhaps most similar to the central portion of TOTO, contains individual sandbars that are narrow and sinuous. The curving bars are generally subparallel. The central portion contains depositional patterns that are different from the southeast and different from TOTO. Sandbars are "amalgamated" into wider features that in detail are formed of sandbars and channels at angles oblique to the trend of the broader feature. Bars are shorter and channels are less throughgoing. A large proportion of the northwest portion of Schooners is filled with a broad expanse of shallow sand.

Sands associated with tidal channels and the numerous islands of the Exumas chain along the western edge of Exuma Sound occur primarily as flood tidal deltas in a linear belt, set back from the platform edge (Harris and Kowalik 1994; McNeil et al. 2004; Harris and Ellis 2009; Harris 2010). In the northern portion of the Exumas included in the current study, lying between Ship Channel Cay to the north and Great Guana Cay to the south, delta lobes extend up to 8 km, averaging 6 km, onto the platform and form a deposit extending 100 km along the platform edge and covering nearly 450 km^2 (Fig. 2C). The islands, often two or three paralleling each other, and the inter-island gaps (= channels) control the distribution of sand. The central portion of the Exumas sand body has a more westerly trend than the surrounding portions, and contains wide channels with associated long, linear sandbars. Flood tidal deltas are more uniformly developed, but still variable, to the north and to the south. The channels are relatively closely spaced in the southern portion, and are regularly spaced but with a different interval in the northern portion.

INTERROGATING THE SAND BODIES AND SANDBARS

Overview

This study attempts to highlight how morphometric interrogation can yield quantitative information on complex depositional environments, in this case sand bodies and sandbars. In order to examine the variation within the sand body, different water-depth intervals are selected and contoured to define polygons that represent individual sandbars and their bar crests. The latter are presumed to correspond to highest-energy well-sorted grainstone deposits, whereas the remainder of the sandbars, by far the largest portion and residing in slightly lower-energy conditions, form less well-sorted grainstones and locally mud-lean packstones.

By simultaneously considering these GIS polygons in unison with the underlying bathymetric DEM, the size, shape, separation distance, connectivity, and three-dimensional form of the sandbars are examined. Centerlines, defined as the sinuous spine of each sandbar and visually interpreted from the DEMs along crests, provide an alternative method of capturing the geometry of the sandbars as compared to the contour-based polygons that describe perimeters. Calculated from these lines were overall length distributions, water depth, spatial density, complexity, and connectivity.

Sand-Body Profiles

Bathymetric profiles derived from the GIS illustrate the variable fill of accommodation space within a sand body. It is a reasonable assumption, based on field observations in all three study areas, that locally the depth of the deepest tidal channels separating the sandbars is a proxy for depth to the Pleistocene. Figure 3 facilitates a direct visual comparison between the sandbars and channels of the three different sand bodies; the figure compares approximately strike-oriented patterns within a central portion of each sand body. Although profiles could be chosen from somewhere in each sand body to identify patterns that are more similar, the exercise here emphasizes variability. Note the drastic differences in sandbar height, width, and spacing, as well as the variability in depth of channels. The spacing between sandbars, as analyzed by Fast Fourier Transform (FFT) along strike-oriented profiles, is different for the three sand bodies and varies within a sand body depending on the nature of the tidal channels between the sandbars. As an example, the dominant frequency of topographic variation determined by FFT across the entire TOTO sand body (Fig. 4A) is 2557 m, whereas the dominant frequency across a portion of the sand body which is dominated by through-going channels (Fig. 4B) is 1713 m. The dominant frequency for TOTO and Schooners calculated over full-length profiles are rather similar (2257 m and 2091 m, respectively). In contrast, the dominant frequency for Exumas is longer at 3553 m, quantifying that which is visually apparent; the topographic highs in this sand body are more lobate and wider than observed in the two other sites. The secondary frequencies delivered by the FFT are however more comparable between sand bodies (TOTO = 852 m, Schooners = 1046 m, and Exumas = 888 m). This is interpreted as the breadth of the channels that separate sandbars; therefore channel breadth seems more consistent between the three sand bodies than the width of the sandbars themselves.

Sandbars and Bar Crests

Contours derived from the DEMs capture the subtle topographic relief across the sand body which is a reflection of the topography created by individual sandbars and channels (Fig. 5B). The sandbars and their bar crests are better delineated when only select contours are draped on the satellite imagery and/or shaded DEM (Fig. 5C–E). Summing the areas within the contour-based sandbars shows that TOTO, Schooners, and Exumas have 421, 113, and 88 km^2 of sandbars, respectively. The portion of each sand body that is occupied by sandbars varies from ~ 15% to 20%, which is a range that seems surprisingly small but can be verified by relooking at Figures 1 and 2 with an emphasis on the tidal channels and other portions of the platform surrounding the sandbars themselves.

The spatial distribution of sandbar areas is variable within each of the sand bodies, as is shown for TOTO in Figure 6A, but the relative proportion of area occupied by bar crests with respect to the area of sandbars is very consistent between the three sites (Fig. 6B). For instance, though the cumulative area of the TOTO sandbars covers nearly five times more area than the Exumas, the ratio of sandbar to bar-crest area for the three sand bodies falls within a narrow range of approximately 3:1 to 4:1. The finding that the proportional representation of the two geobodies is consistent is somewhat surprising, especially given the differences in morphology between the sand bodies.

Power-law scaling between patch area and frequency of occurrence has been observed in carbonate environments (Drummond and Dugan 1999; Rankey 2002; Harris and Vlaswinkel 2008; Purkis and Kohler 2008; Purkis et al. 2005; Purkis et al. 2007; Purkis et al. 2010; Fullmer et al. 2010). This property is useful in providing an empirical function linking the prevalence of small geobodies in a landscape to the scarcity of large ones. Evidence for power-law scaling is a linear relationship in a log-log plot of patch area versus patch frequency. The power law decrees that the

→

FIG. 3.—Strike-oriented bathymetric profiles derived from the GIS for TOTO, Schooners, and Exumas. Profiles are same horizontal scale; vertical scales differ, and exaggeration is very high.

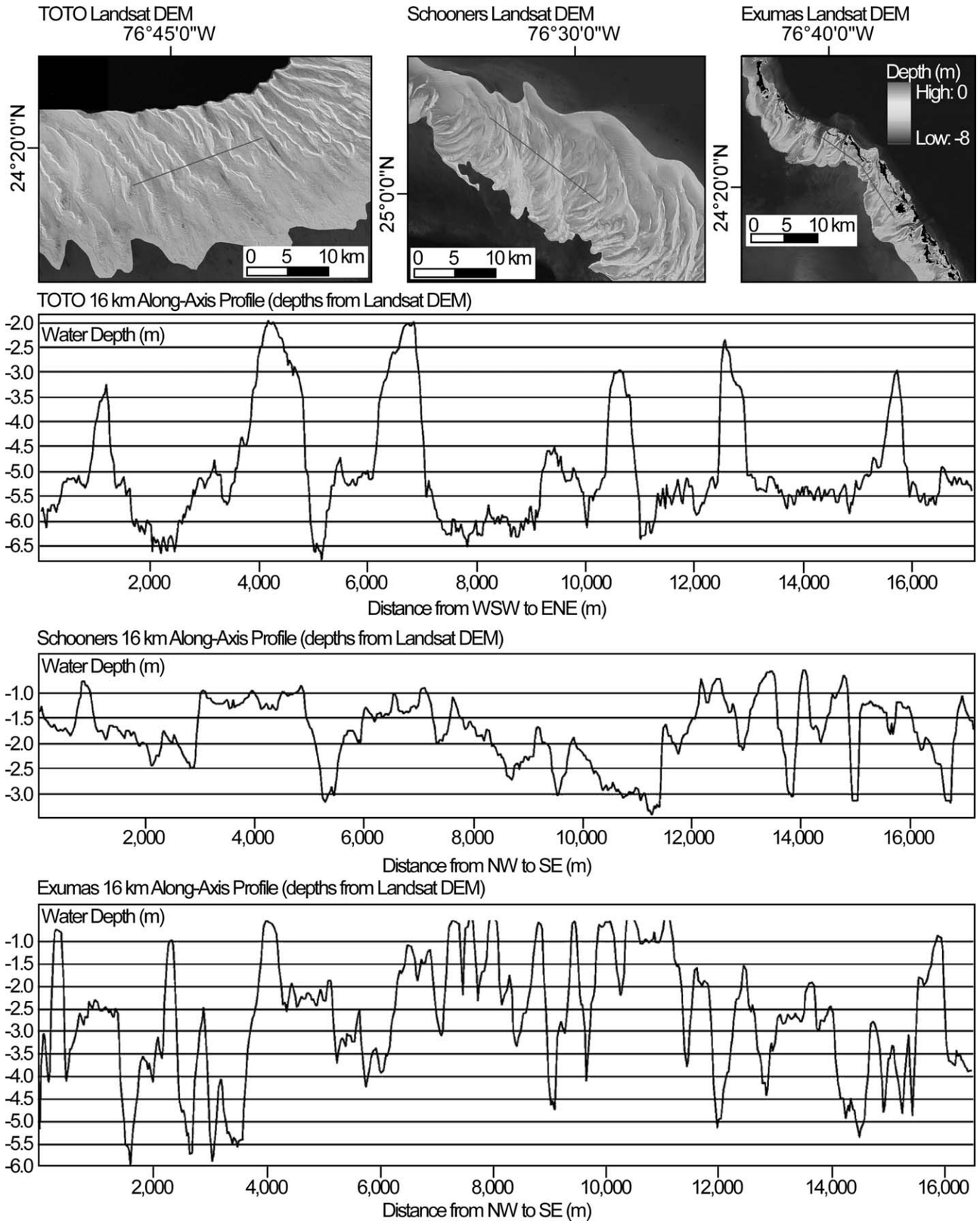
TOTO Landsat DEM
76°45'0"W
24°20'0"N
0 5 10 km
Schooners Landsat DEM
76°30'0"W
25°0'0"N
0 5 10 km
Exumas Landsat DEM
76°40'0"W
24°20'0"N
Depth (m)
High: 0
Low: -8
0 5 10 km
TOTO 16 km Along-Axis Profile (depths from Landsat DEM)
Water Depth (m)
-2.0
-2.5
-3.0
-3.5
-4.0
-4.5
-5.0
-5.5
-6.0
-6.5
2,000
4,000
6,000
8,000
10,000
12,000
14,000
16,000
Distance from WSW to ENE (m)
Schooners 16 km Along-Axis Profile (depths from Landsat DEM)
Water Depth (m)
-1.0
-1.5
-2.0
-2.5
-3.0
2,000
4,000
6,000
8,000
10,000
12,000
14,000
16,000
Distance from NW to SE (m)
Exumas 16 km Along-Axis Profile (depths from Landsat DEM)
Water Depth (m)
-1.0
-1.5
-2.0
-2.5
-3.0
-3.5
-4.0
-4.5
-5.0
-5.5
-6.0
2,000
4,000
6,000
8,000
10,000
12,000
14,000
16,000
Distance from NW to SE (m)

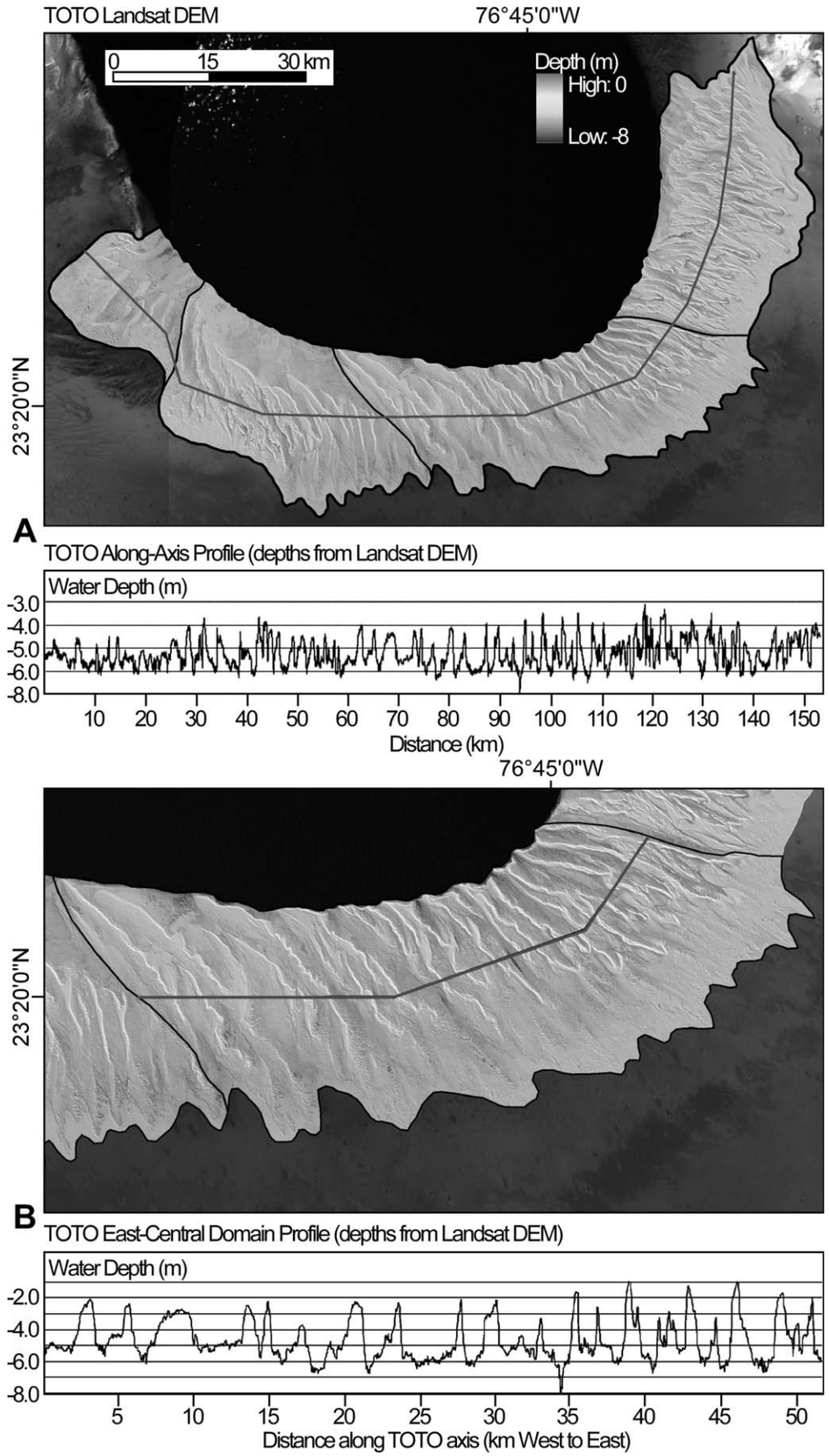

FIG. 4.—**A)** Strike-oriented profiles along the entire length of the TOTO sand body, and **B)** across only the southern portion to highlight sandbar variability.

frequency of patches decreases with increasing patch area according to

$$f = e^{\beta} \times A^{m}, \quad (1)$$

where f is the number of patches having area A, m is the slope of the regression line (negative), and β is the y intercept. The implication of the existence of power-law scaling is that not only do patches become more abundant with decreasing area (or length); they do so at a predictable rate. In contrast to the body of literature on reefal landscapes, the frequency-area distribution of sandbars depicted by Figure 7 are clearly non-linear in this log-log plot and hence not power-law distributed. The trend of the data is however informative: small geobodies are more prevalent than large, and for the case of the Exumas and Schooners, the frequency-area distributions of sandbars and crests are highly comparable. TOTO follows a markedly different trajectory since its bars and crests are approximately one order of magnitude larger than Exumas and Schooners across the greater part of the size spectrum for the three sand deposits.

Figure 7A serves to compare the frequency-area distributions of the Schooners sandbars to three model populations; a power-law fit through areas of 10,000 m^2 to 1 km^2, a random Gaussian distribution for the area-span of the Schooners population, and a negative exponential distribution. The latter, which returns an r^2 of 0.97 and is a linearly curved distribution, clearly approximates the Schooners dataset very well. By contrast, a power law offers a reasonable fit to this population only over a narrow span of areas (10^4 through 10^6 m^2). Beyond 10^6 m^2, the actual data series bends beneath the power-law trend, caused by an underrepresentation of large geobodies as compared to the power-law prediction. The exponential model is further explored in Figure 7B and C, where it is fitted through the frequency-area distributions of the sandbars and bar crests for the three sand bodies studied. As depicted in the figure, high values of r^2 in each case show the exponential model to robustly fit to the real-world data. Though for several of the plotted populations there is some divergence of the model at the large end of the series (e.g., TOTO crests, Fig. 7C), these large geobodies are comparatively rare in the dataset and an excellent fit is returned at the smaller sizes, such that the r^2 is high (0.99 in the case of the TOTO crests). The model used to create the exponential distributions is that detailed, among others, by Wilkinson and Drummond (2004) and McElroy et al. (2005), namely

$$Rank(Ai) = N \times e^{-(pA_i)^{0.5}}, \quad (2)$$

where *Rank* is the size rank of the ith area (A) within the population and N is the total number of elements in the series and p is calculated per

$$p = \left(\frac{N0.5\pi}{T}\right)^{0.5}, \quad (3)$$

where T is the sum of Ai through j.

For each dataset, application of Equations 2 and 3 requires only the total number of areas in each population to be modeled and total area occupied by that population. The model yields a negative exponential distribution of geobody areas, that is, a frequency distribution where a linear decrease in probability of encounter (i.e., EP) is accompanied by an exponential decrease in geobody area. A power-law, by contrast, would be represented by an exponential decrease of both variables. Populations that adhere to the exponential trend have been reported for the distribution of lithofacies thicknesses in ancient carbonate strata (Drummond 1999; Wilkinson et al. 1997, 1998, 1999; Carlson and Grotzinger 2001; Burgess and Wright 2008), synthetic models of carbonate accumulation (Drummond and Dugan 1999), as well as for frequency-extent distributions of contemporary carbonate facies in plan-view mosaics (Drummond and Dugan 1999; Wilkinson and Drummond 2004). Framed by these works, the exponential scaling for the Bahamian sand deposits reported by this study is of considerable relevance, as is the observation that these grainy geobodies are not power-law distributed, a common property for plan-view mosaics of modern carbonates (Drummond and Dugan 1999; Rankey 2002; Harris and Vlaswinkel 2008; Purkis and Kohler 2008; Fullmer et al. 2010; Purkis et al. 2005; Purkis et al. 2007; Purkis et al. 2010).

Like the mathematical simplicity of power scaling (Equation 1), an exponential distribution is also describable by a generic set of equations (Equations 2 and 3). Referring to Equation 1, a power-law distribution is "scale invariant" since frequency (or EP), regardless of magnitude, can always be obtained by scaling A by a constant factor m. Hence, the frequency-area distribution of any population scaling as such is predictable. By contrast, an exponential distribution does not possess a constant scaling factor. However, while not scale invariant, the distribution is again predictable since the scaling factor diminishes at a constant rate with increasing A. Comparable to m in a power law, this failure rate, p, is a defining statistic of the exponential population. As shown in Figure 7B and C, the higher the p, the more acute the roll-off of the model at the large ends of the series.

Shape of Sandbars

Shape parameters are developed for the sandbars by applying the formulas (Equations 4 through 7) to measurements of the sandbars. The metrics calculated were form factor (*FF*), sinuosity (*S*), aspect (*As*), and roundness (also termed elongation) (*R*):

$$FF = \frac{4\pi A}{\mathrm{Pr}^2}, \quad (4)$$

$$S = \frac{L - DMG}{L}, \quad (5)$$

$$As = \frac{L - W_a}{L}, \quad (6)$$

$$R = \frac{DMG - W_m}{DMG}, \quad (7)$$

where A is the area of a sandbar polygon, Pr is the perimeter, L is length, W_a and W_m are average and maximum widths, respectively, and DMG is "distance made good." These measurements are depicted in Figure 8A.

As an illustration of the spatial distribution of sandbar shape, form factor is shown for the TOTO sandbars in Figure 8B. Form factor as determined here follows that of Russ (1999), wherein more circular shapes have uniquely high values of form factor, with a value of 1 being a perfect sphere. All three sand bodies have sandbars that are dominated by low form factors, corroborating and quantifying the visual observation from imagery of the elongate nature of the bars. Quantifying the shape using the form factor and other shape parameters facilitates a more direct comparison of sandbars within and between the three sand bodies. For 517 sandbars analyzed from the three sand bodies, the mean and standard deviation for form factor is 0.30 $\pm$ 0.17, sinuosity is 0.16 $\pm$ 0.16, aspect is 0.83 $\pm$ 0.11, and roundness is 0.64 $\pm$ 0.23. Overall, sandbars from TOTO are slightly more elongated than from the other two areas, but there is a surprising similarity in shape of individual sandbars between the three areas given that the sand bodies themselves have differences.

A systematic behavior is observed between the area of each sandbar and its shape for each of the three sand bodies. Figure 8C demonstrates a clear trend of greater elongation with increasing sandbar area. That is, small sandbars tend to be rounded sandbars, whereas large (> 1 km^2) are exclusively elongate. This relationship is consistent with observations of facies sizes and shapes reported from reefal environments, which also

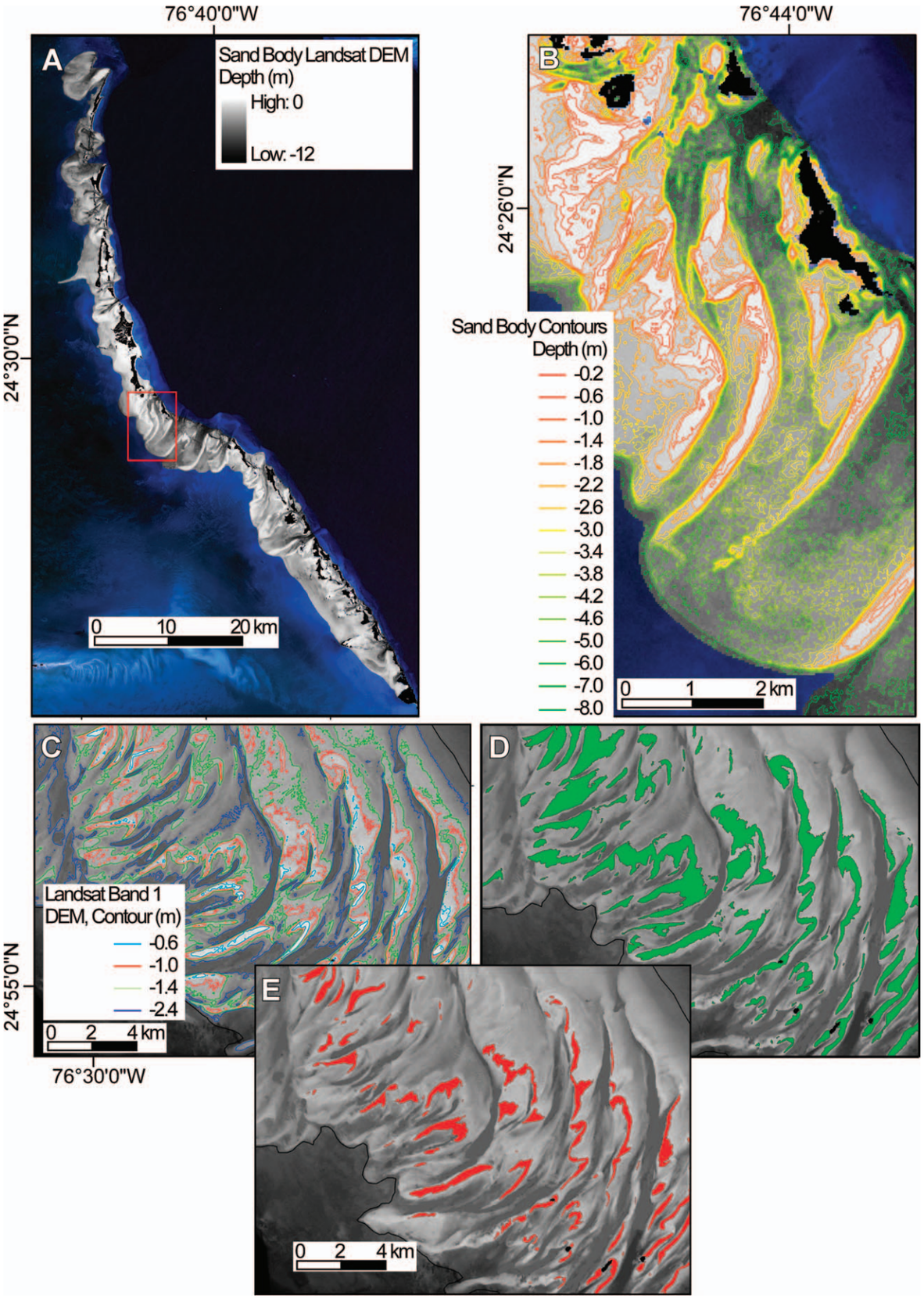
76°40'0"W
76°44'0"W
24°30'0"N
24°26'0"N
24°55'0"N
76°30'0"W
A
Sand Body Landsat DEM
Depth (m)
High: 0
Low: -12
0 10 20 km
B
Sand Body Contours
Depth (m)
-0.2
-0.6
-1.0
-1.4
-1.8
-2.2
-2.6
-3.0
-3.4
-3.8
-4.2
-4.6
-5.0
-6.0
-7.0
-8.0
0 1 2 km
C
Landsat Band 1
DEM, Contour (m)
-0.6
-1.0
-1.4
-2.4
0 2 4 km
D
E
0 2 4 km

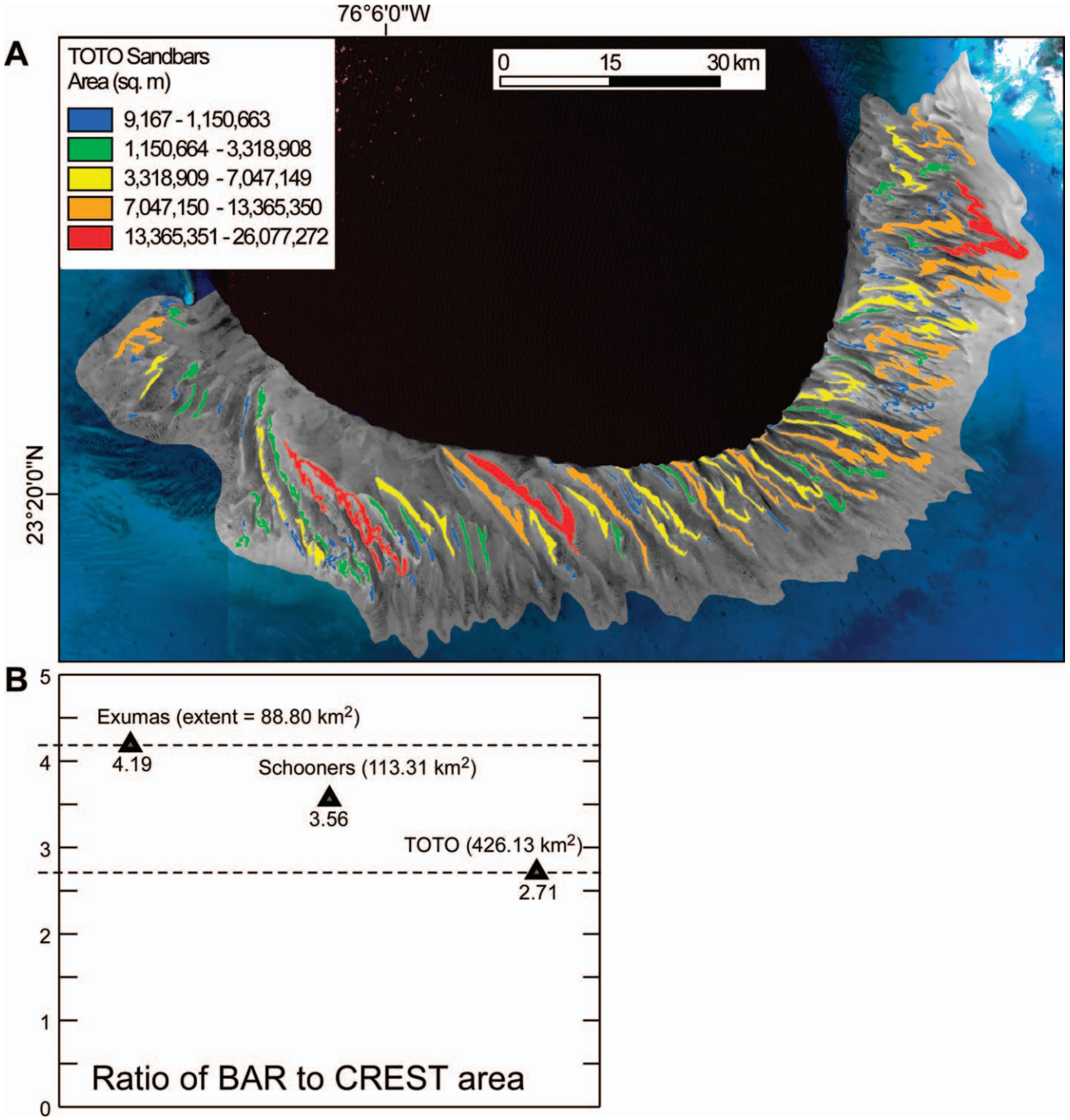

FIG. 6.—**A)** Area distribution of sandbars for the TOTO sand body are displayed on the shaded DEM. **B)** Ratio of areal extent of sandbars versus bar crests for the three sand bodies. The total extents of the sandbars are given in brackets.

←

FIG. 5.—**A)** Red outline shows subarea from the Exumas enlarged in Part **B**, where contours of the bathymetric DEM are draped over the Landsat color image to delineate details within the sand body. **C)** Select contours, in this case from the Schooners bathymetric DEM, delineate individual sandbars highlighted with green polygons in Part **D**, and bar crests are indicated by red polygons in Part **E**. Contours used to define the sandbars are distinct and isolated, at the deepest depths of the feature before it merges with other sandbars, and visually represent the closed shape of the sandbar. The contours representing bar crests are chosen based on continuity, size, and separation from the deeper individual sandbars.

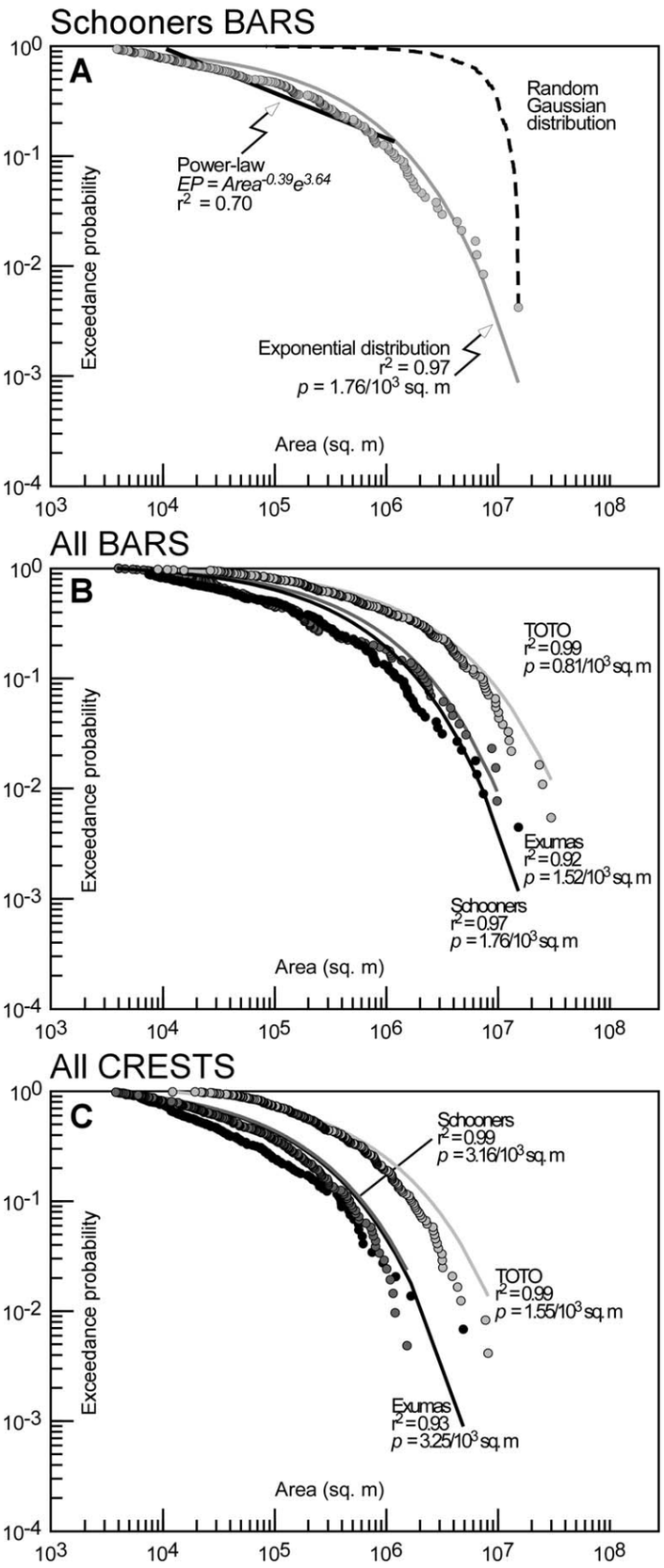

FIG. 7.—Frequency-area distributions of sand bodies. **A)** Comparison of the EP vs. area distribution of the Schooners sandbars (circles) with a random Gaussian population (broken black line) and an exponential distribution (solid gray line). The latter clearly fits the dataset well, whereas the power law (solid black line), does not. For each of the three sand bodies, Parts **B** and **C** sees the exponential model calculated for sandbars and bar crests, respectively. These distributions, like the exponential model with which they are plotted, exhibit a steady curve throughout with no linear segments. Axes are log-scale, and *p* denotes the failure rate of each exponential model.

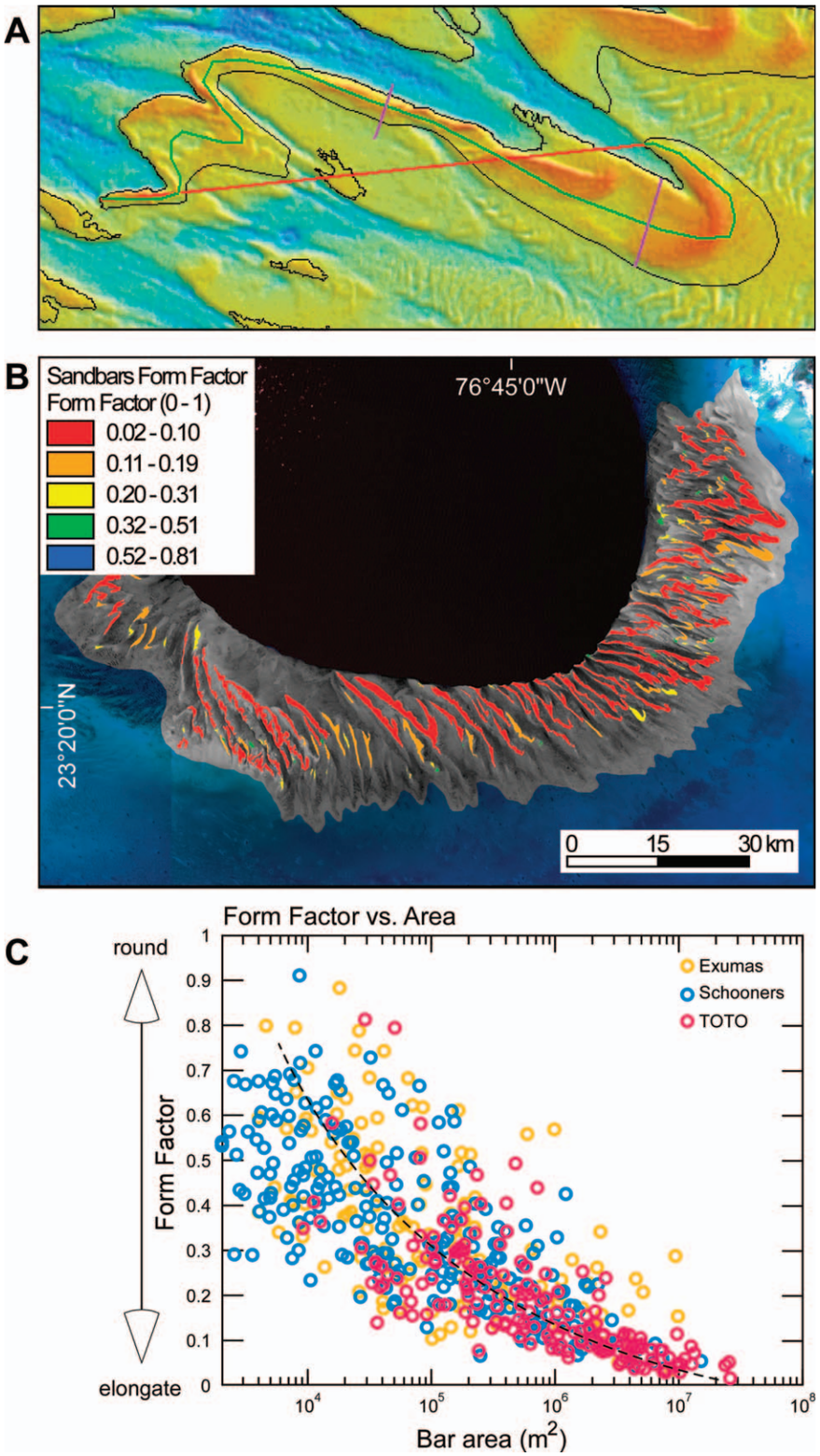

FIG. 8.—**A)** Example of measuring total length (*L*, green line), distance made good (*DMG*, red line), maximum width (W_m, longer purple line) and estimated average width (W_a—shorter purple line) for an irregular-shaped sandbar. **B)** Form factor is shown for sandbars on the shaded DEM for the TOTO sand body. **C)** Plot showing area of sandbars (log) vs. their form factor, color-coded by sand body.

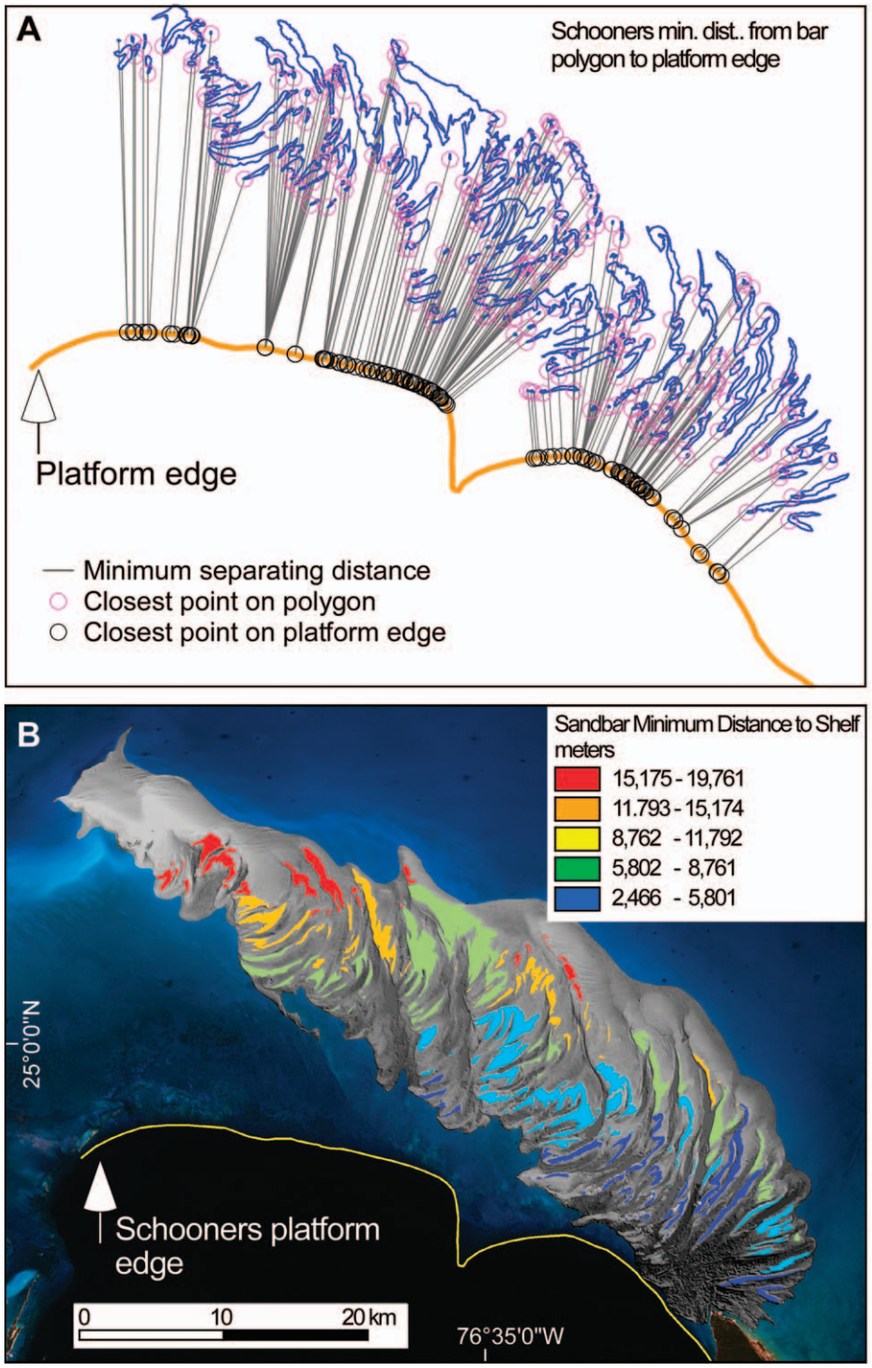

FIG. 9.—Using Schooners as an example, **A)** minimum distance to the platform edge from each sandbar polygon, and **B)** the spatial distribution of these distances for each polygon on the shaded DEM.

show a propensity for round-small and elongate-large geobodies (Purkis et al. 2007; Harris and Vlaswinkel 2008).

Separation Distance

The northwest portion of the Schooners sand body is substantially farther from the platform edge than the southeast portion, so a striking pattern emerges which arcs across the sand body when the sandbars are analyzed with respect to their distance from the platform edge (Fig. 9). The setback distance of sandbars from the platform edge was calculated using code written in the MATLAB language. This algorithm tallied the minimum separating distance between a manually digitized line describing the platform edge, to the closest point on every sandbar polygon. Particularly strong trends are observed at Schooners when this offset distance is compared to the mean and variance in depth of the sandbars. In Figure 10A, the distance metric is color-coded to separate sandbar polygons found in close, intermediate, and far proximity to the platform edge (x axis) versus mean water depth determined from the DEM for each Schooners sandbar (y axis). The trend shows the tops of sandbars in close proximity to the edge to be, on average, deeper than those found more

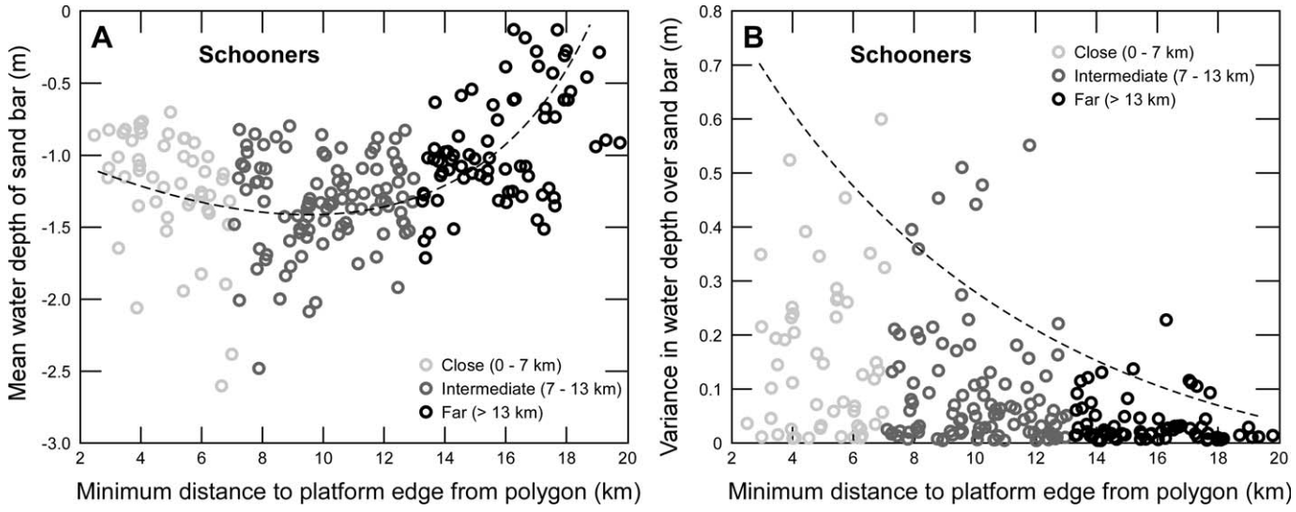

FIG. 10.—Plots showing minimum distance to the platform edge from each sandbar polygon at Schooners vs. **A)** mean water depth and **B)** variance in water depth of the sandbars, color-coded by setback distance.

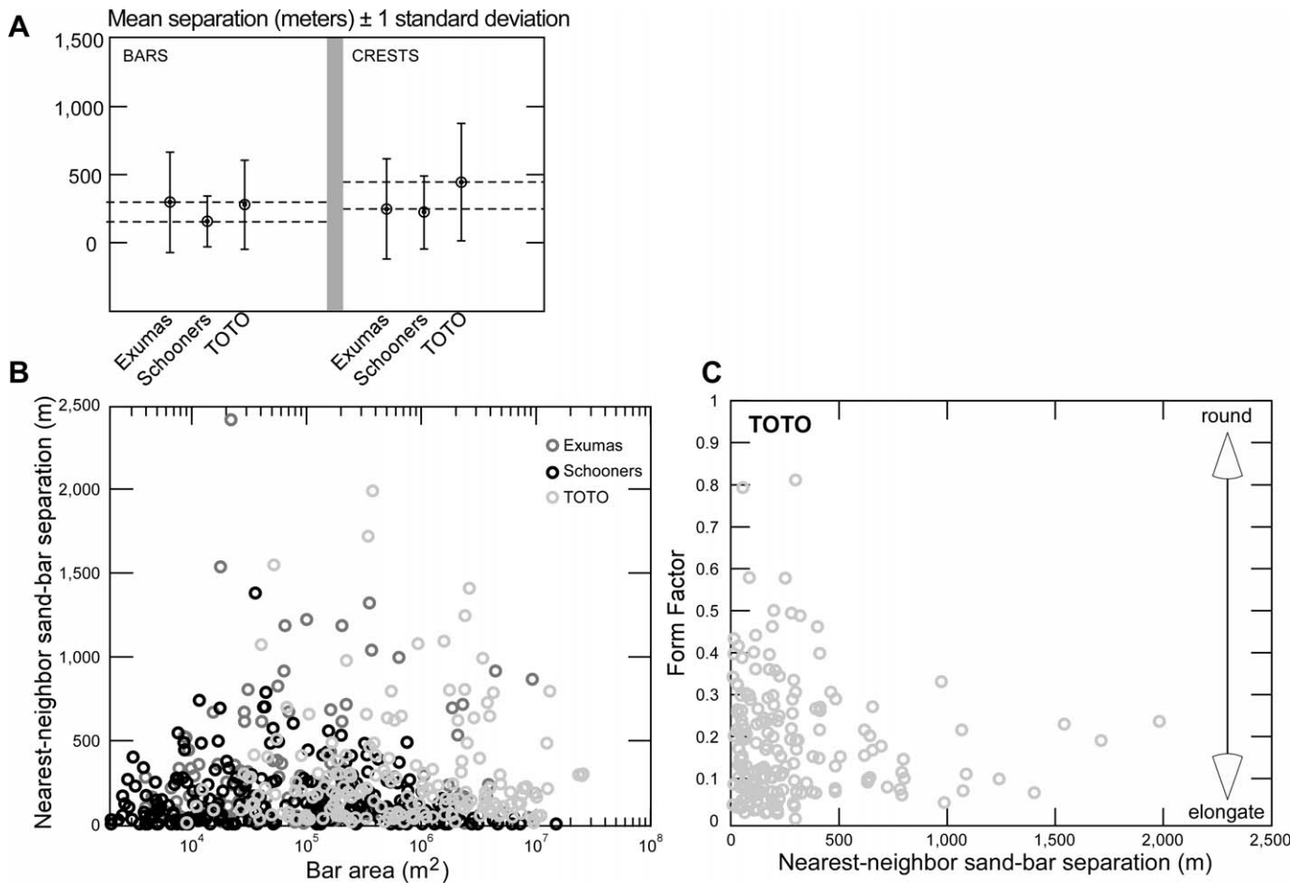

FIG. 11.—**A)** Mean and variance of minimum separation distance between sandbars and bar crests across the three sand bodies. **B)** Plot of area of each sandbar versus the minimum distance to its nearest neighbor shows that size has no bearing on the separating distance. Distance is measured perimeter-to-perimeter. **C)** Plot showing nearest-neighbor separation distance vs. form factor for sandbars from the western portion of TOTO.

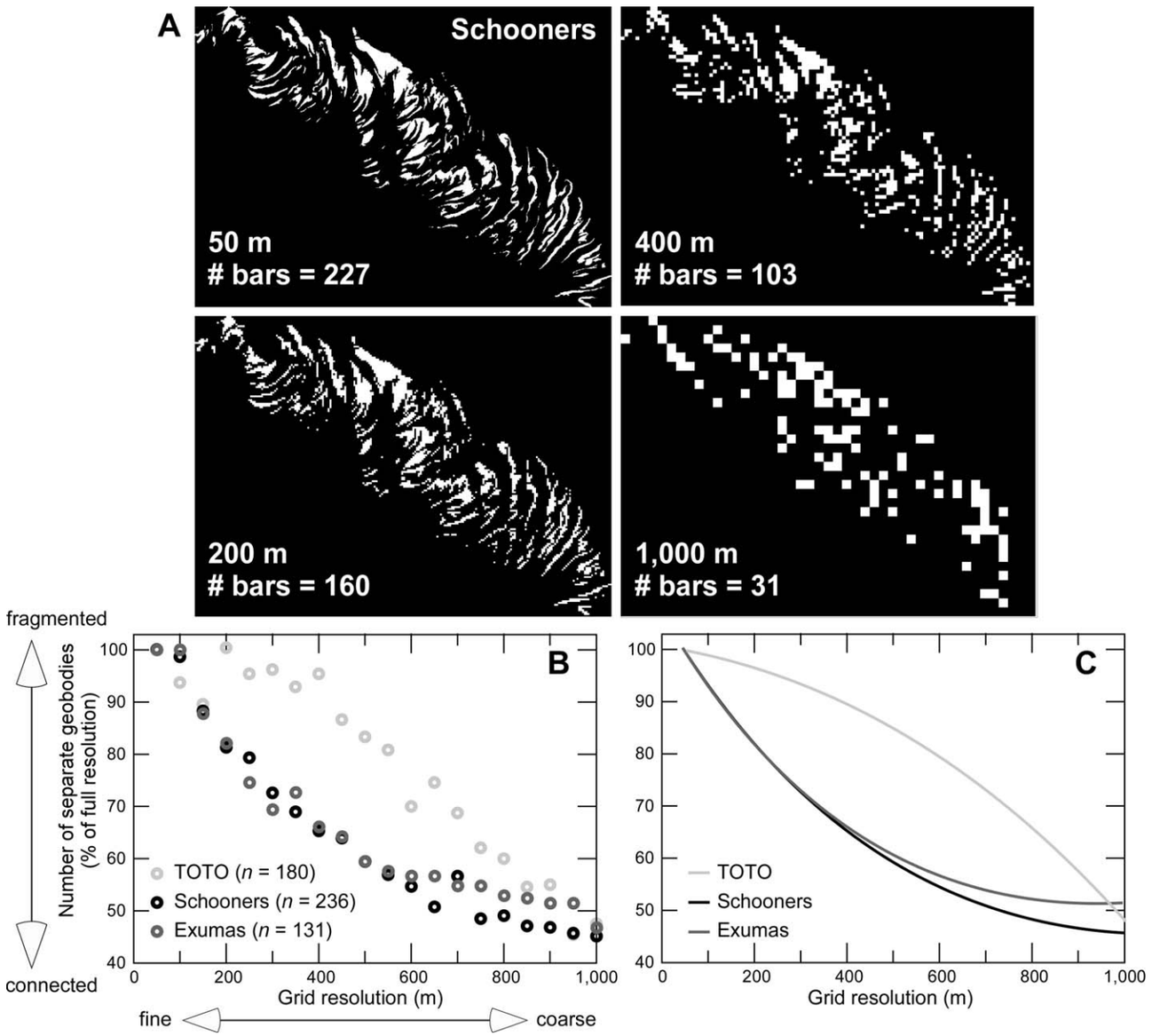

FIG. 12.—**A)** The impact of coarsening the resolution at which an area is considered is illustrated by the sandbars of the Schooners sand body, here depicted as a binary image where sandbars are white and background is black. **B)** Plot showing the decrease in connectedness of the three sand bodies as a function of resolution. The *x* axis depicts the varying resolutions to which each system was spatially down-sampled. The *y* axis is the number of discrete sandbars remaining after each coarsening of the dataset, expressed as a percentage of the total number in the raw dataset (*n* given in key). **C)** The first-order trends.

distally. Systematic behavior is also observed when considering variance in water depth atop the sandbars as a function of setback distance (Fig. 10B). The greatest variances in depth typify sandbars in close proximity to the platform edge, which we also know to have the deepest tops.

A modification of the algorithm used to interrogate the distance to the platform edge was used to quantify the minimum separation distance between sandbars. The spatial patterns of sandbar separation vary between the three sand bodies and indeed within each sand body, but there is robust and systematic behavior in the mean and variance of the separation distance between sandbars and bar crests which are shown in Figure 11A to group within narrow thresholds. That is, the mean separating distances between geobodies across the three sand bodies is similar, despite the varying depositional settings and morphologies. The previously discussed secondary frequencies, determined by FFT, for the three sand bodies also shows that the average separation between sandbars (breadth of the channels) falls within a narrow threshold of only a few hundred meters.

Consistent behavior is also seen for the three sand bodies in the relationship between sandbar separating distance and sandbar area, whereas in Figure 11B no clear trend between these variables is recognized. We conclude that the size of a sandbar has no bearing on the separating distance to the nearest neighbor. In contrast, systematic trends are defined when separation distance is plotted against the variance in water depth atop each sandbar from all three sand bodies, wherein closely spaced sandbars show the greatest variance in depth. More separated sandbars have a distinctly lower variance in water depth, but they may or may not be close

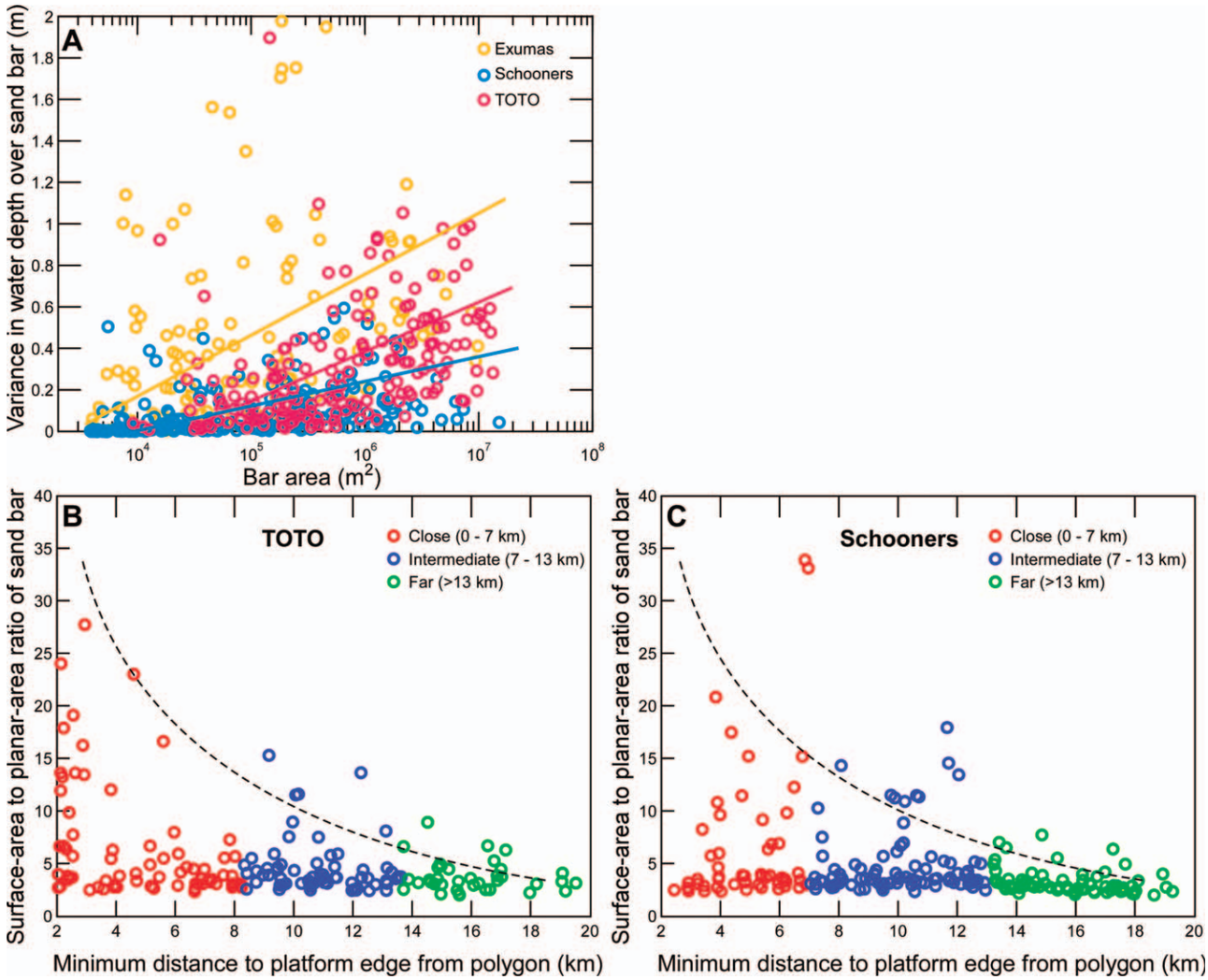

FIG. 13.—**A)** Area of each sandbar versus variance in its water depth. The variance in depth of the DEM can be considered a proxy for consistency in thickness of the sandbar. Plots showing minimum distance of sandbars to platform edge vs. surface-to-planar ratio for **B)** TOTO and **C)** Schooners sand bodies.

to the platform edge. Sandbar separation also performs predictably with respect to shape. In Figure 11C, which cross-plots these variables for a portion of TOTO, more rounded bars, as quantified by the form factor, are found within close proximity to one another. Those separated by great distance have a tendency to be elongate.

Bar Packing

We use the term "bar packing" to describe how the perception of connectivity between sandbars in each sand body changes with the resolution at which the system is considered. The connectivity between sandbars for the Schooners sand body is considered in Figure 12A, which shows the number of discrete sandbars in the sand body is 227 when considered with a grid resolution of 50 m. As the grid is successively coarsened, the number of separate sandbars decreases, reaching only 31 at a resolution of 1,000 m. Figure 12B and C takes the bar packing strategy further, identifying differences in behavior for the three sand bodies. While the decrease in connectivity for Schooners and Exumas behave in a nearly identical fashion, TOTO is markedly different, retaining a lower level of bar connectedness through coarsening than the other two sand bodies. Compared to the raw data and even when viewed at the coarse resolution of 500 m, the degree of connectedness for TOTO is increased by only 15%. At this level, Schooners and Exumas have both become $\sim$ 40% more interconnected. Such experimentation is informative in that it predicts how the sedimentary system might appear under, for example, the limited spatial resolution of a coarse-scale satellite image or seismic data. When faced with the audits of depositional anatomy that satellite and seismic can provide, it is valuable to be able to appraise "true" connectivity between geobodies, as opposed to that "perceived" by these two resolution-limited remote sensing technologies. Though beyond the scope of this study, it would be worthwhile to repeat the assessment of bar packing using meter-scale satellite imagery such as provided by IKONOS, QuickBird, or WorldView-2.

Three-Dimensional Form of Sandbars

A sandbar with a high variance in water depth over its top is considered to have a rough topographic surface, and hence is reasonably interpreted

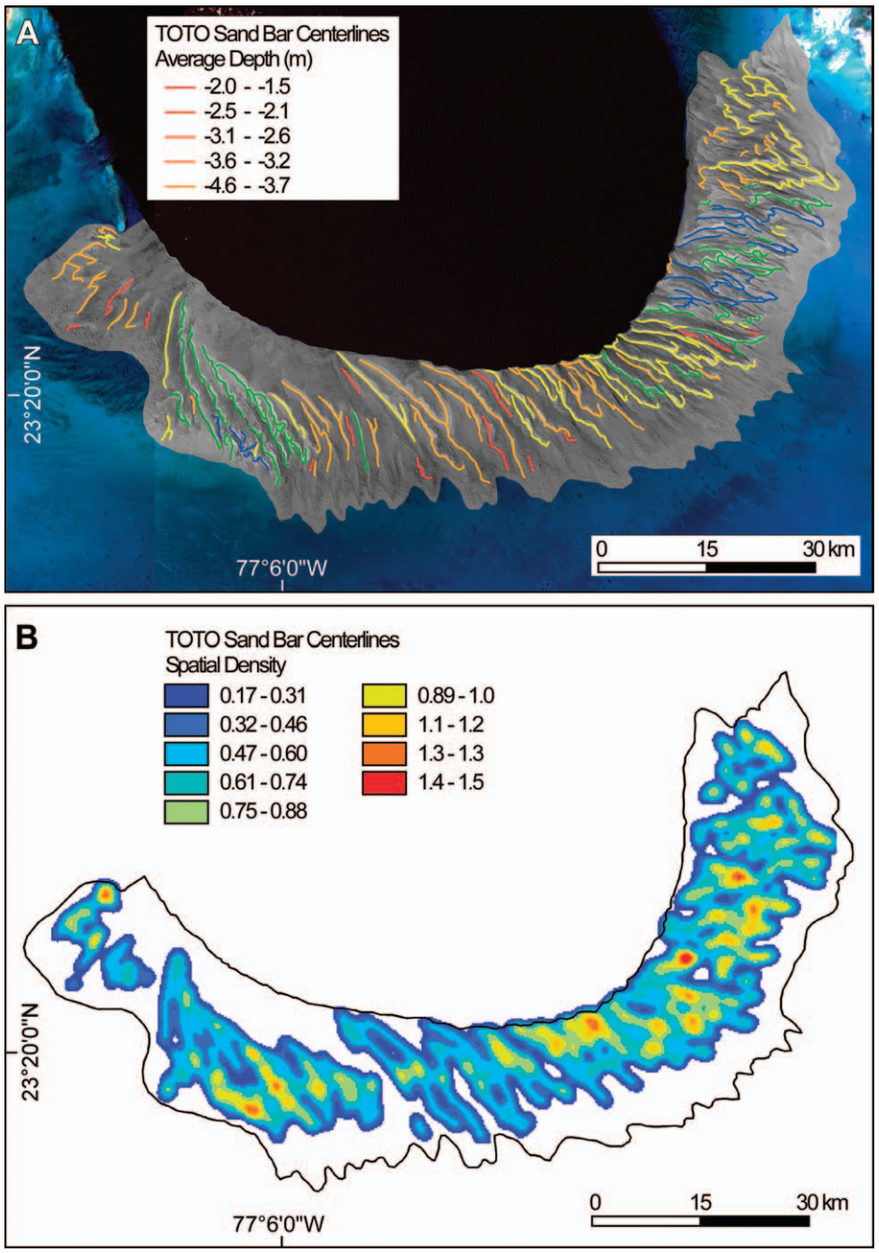

FIG. 14.—**A)** Centerlines of sandbars within the TOTO sand body are superimposed on the shaded DEM and color coded by their average water depth. Centerlines can extend beyond the boundary of sand bar polygons, resulting in deeper measurements being included in the calculation of average water depth of centerlines compared with that calculated for the associated sand-bar polygon. **B)** The density of centerlines; units are centerlines per square kilometer.

to have a great variation in thickness. As depicted in Figure 13A, there is a clear trend such that the sandbars with the roughest surfaces (i.e., most thickness variation) tend to be of greatest area. The positive relationship is consistent between the three sand bodies. An efficient means with which to appraise the complexity in three-dimensional form for the sandbars is through calculation of the ratio of surface to planar area. This is achieved by taking the area of the surface, as defined by the DEM that envelops each sandbar, and dividing it by the flat planar area of the same sandbar. The surface value is based on the volume of the bar, and that is controlled by its vertical height (as calculated from the Landsat DEM) and the width of the sandbar. The greater the bar's depth range, the greater the surface value. The narrower the sandbar, the smaller the planar value; therefore, a narrow sandbar that has a large vertical height will have the highest surface/planar ratio. A sandbar with little topographic relief yields an index approaching 1, with more complex and rough sandbars yielding higher values. Figure 13B and C shows the surface-to-planar ratio of the sandbars to be well behaved with respect to the setback distance from the platform edge. As demonstrated in this figure for TOTO (Fig. 13B) and Schooners (Fig. 13C), the sandbars that attain the highest surface-to-planar ratio values are typically in proximity to the seaward margin of the sand body and, as visually apparent on the Landsat images and DEMs, their geometry is linear and elongated.

Centerlines

Centerlines are also developed for the sandbars in order to provide methods of capturing information that are alternative to that of the contour-based sandbar polygons. Centerlines are visually interpreted along

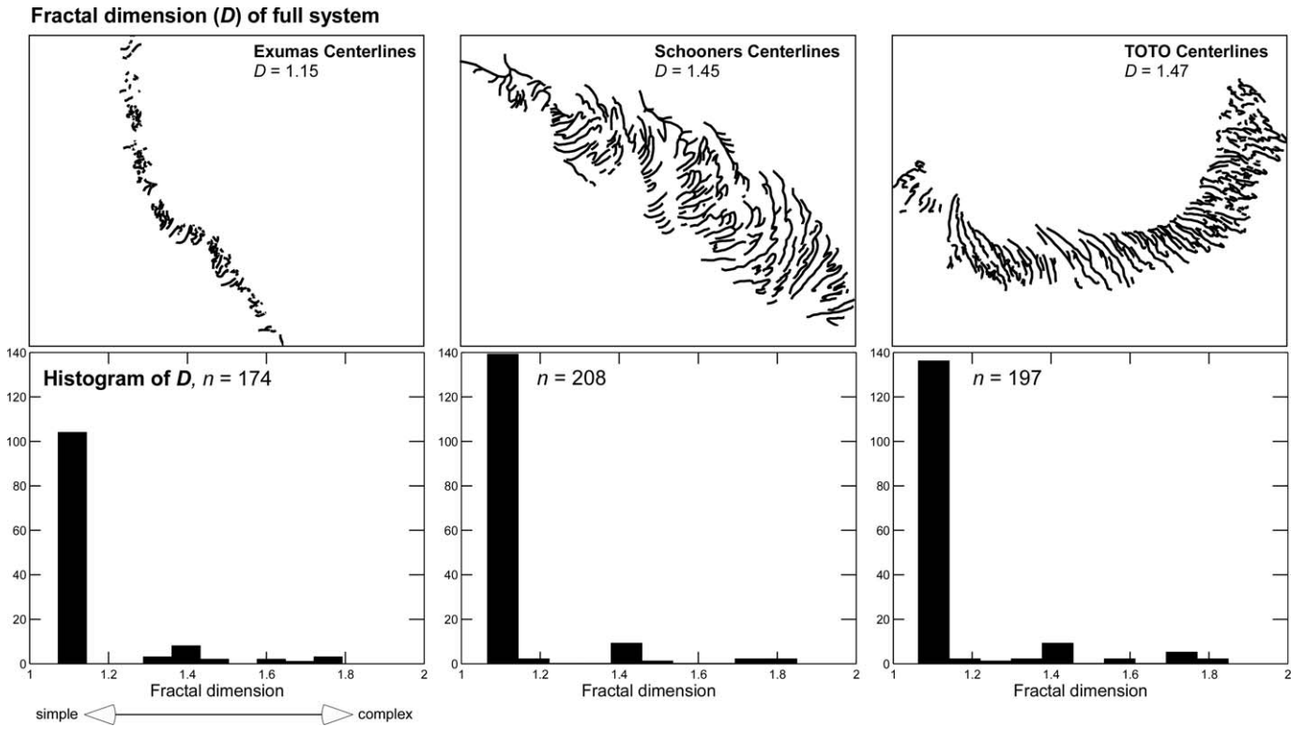

FIG. 15.—Top row depicts centerlines for sandbars in each of the three sand bodies and the overall complexity of each network as measured by the fractal dimension (D). The bottom row shows the complexity of each individual centerline as a histogram.

the crests of the sandbars using the bathymetric DEM where subtle topography was highlighted by low-altitude illumination (shaded DEM) and the color Landsat TM and ETM+ images. This study was relatively conservative with centerline delineation, focusing on sandbars delineated by the contour method and in some cases extending the length of sandbars. The centerlines can be analyzed for their length, depth, complexity, density, or connectivity. As an example, the total length of centerlines for TOTO, Schooners, and Exumas is 1079, 534, and 245 km, respectively. An average water depth can be attached to the centerlines as an attribute based on the bathymetric DEM and is shown for TOTO in Figure 14A. A large concentration of shallow sandbars occurs in the northeastern portion of TOTO, whereas deeper sandbars are found in the southern portion.

Kilometer-scale concentrations of high centerline density are scattered throughout the TOTO sand body (Fig. 14B), but there is generally a higher density in the eastern half of the sand body than the western half. TOTO and Schooners, the two sand bodies with few islands, have very similar centerline density (32% and 35%, respectively), whereas the island-rich Exumas has a relatively lower centerline density (21%). Visual inspection of the Landsat and derived DEMs for the three sand bodies corroborates that sandbars develop differently in areas with and without islands. Sandbars generally tend to be elongated, with sharper crests and extents that plunge into deeper water, where there are no islands. Sand deposits in the Exumas are lobe-shaped, tend to be flattened, and are concentrated near tidal channels whose spacing is dictated by island development.

The fractal dimension (D) describes the fractal complexity of an object, which for a 2-D line such as this study's sandbar centerlines, scales between 1.0 and 2.0. On this scale, a dimension of 1.0 means totally smooth, while tending towards 2.0 implies increasing fractal complexity, as would be observed for intricate, sinuous centerlines. The complexity of the centerlines for the three sand bodies is measured using a box-counting algorithm as detailed by Purkis et al. (2005) and Purkis et al. (2007). The centerlines in this study are considered in two different ways: (1) all centerlines are considered simultaneously as a composite, as depicted in the top row of Figure 15, where one value of D is determined for each of TOTO, Schooners, and Exumas; and (2) each individual centerline is separately box-counted for its fractal complexity to produce the histograms of fractal dimensions shown in the bottom row of Figure 15. While Schooners and TOTO are of almost identical fractal complexity, Exumas is considerably less complex (D = 1.15 vs. 1.45 and 1.47). All sites show the same pattern—simple centerlines are by far the most prevalent, while each site displays a small number of highly complex and convoluted bar lines (< 50, or $\sim$ 25% of the total). That is, the tendency for the formation of sinuous and intricate centerlines, a proxy for well-sorted grainstone crests, is similar between the sand bodies, suggesting similar formative mechanisms at play in each setting.

Connectivity

Beyond considering the complexity of centerlines, the degree of connectivity between the individual centerline segments for each sand body yields different insight. Figure 16A shows three different ways of considering centerline connectedness using a flood tidal delta lobe in the Exumas as the example. A "threshold of connectedness" can be set which serves to render any discrete centerlines that are separated by a distance less than the threshold to become amalgamated into a single composite centerline. Imposing this threshold is analogous to considering how the connectedness of the sandbars would increase if, for example, the rate of grain production was to increase and infill the channels that now separate individual sandbars. In the figure, the eight raw centerlines become assimilated into five composite centerlines when a threshold of connectedness of 70 m is imposed, and are assimilated into a single composite with a 100 m threshold, with the relevance being that the

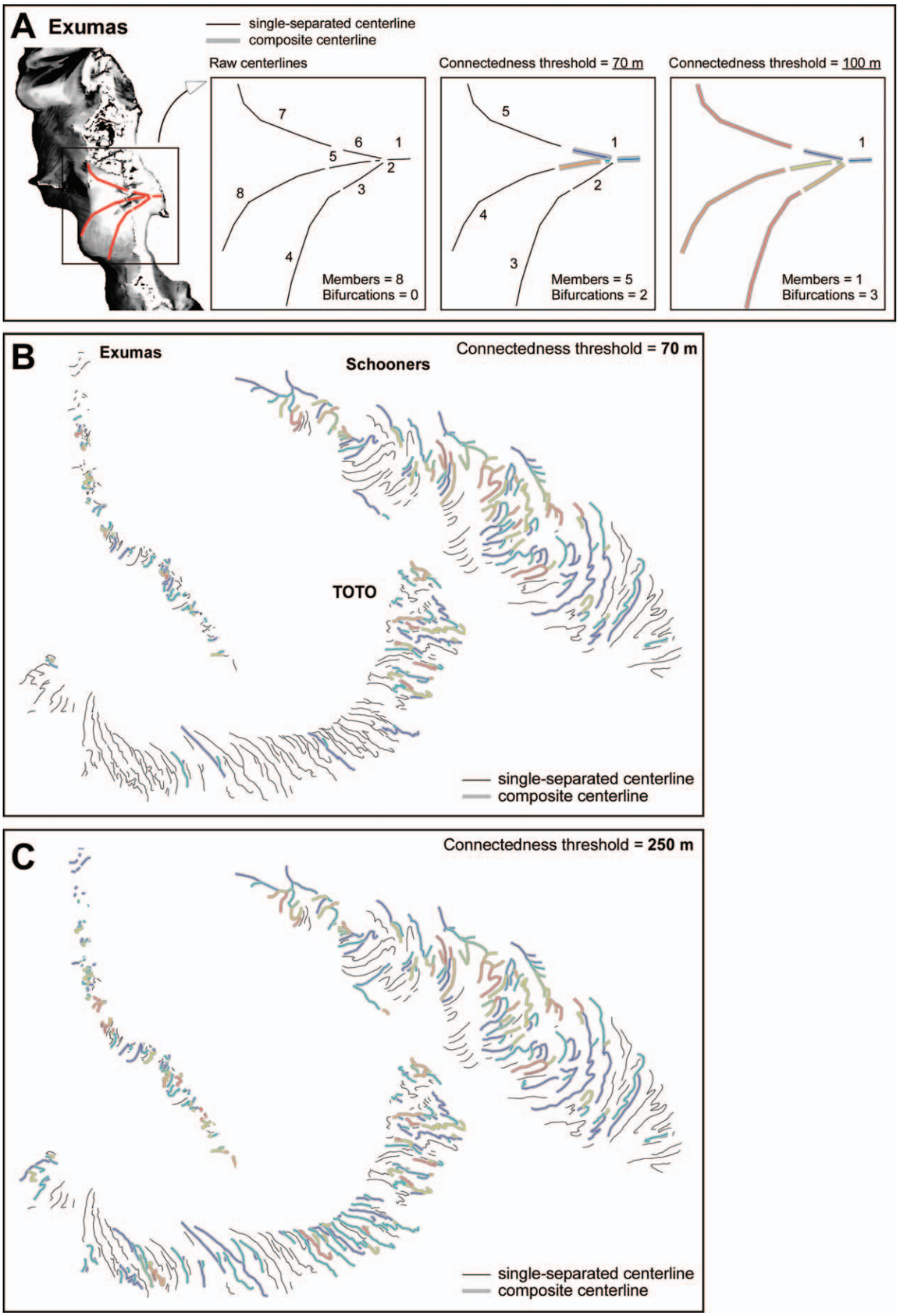
A Exumas
single-separated centerline
composite centerline
Raw centerlines
Connectedness threshold = 70 m
Connectedness threshold = 100 m
Members = 8
Bifurcations = 0
Members = 5
Bifurcations = 2
Members = 1
Bifurcations = 3
B
Exumas
Schooners
TOTO
Connectedness threshold = 70 m
single-separated centerline
composite centerline
C
Connectedness threshold = 250 m
single-separated centerline
composite centerline

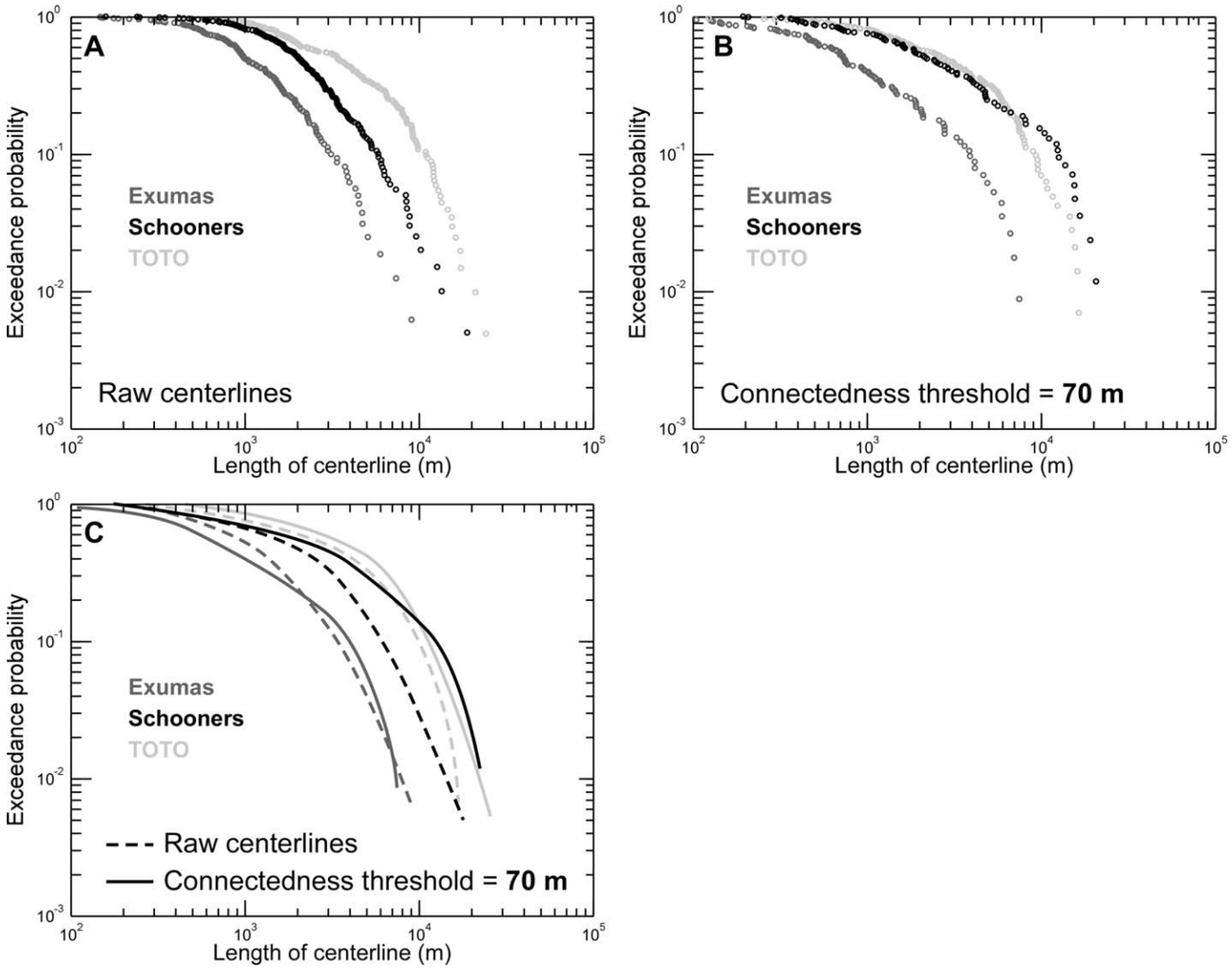

FIG. 17.—Exceedance probability (EP) versus length of centerlines for the three sand bodies. **A)** The EP-length relationship for centerline lengths of the raw dataset; **B)** EP vs. lengths for the three domains after a connectedness threshold of 70 m has been imposed; **C)** the trends of both (raw dataset as a broken line, coalesced centerline distribution as a solid line).

interconnectedness of the composite centerlines is much greater. Furthermore, imposition of the 100 m threshold has served to increase the complexity of this centerline, because the composite now has three points of bifurcation. This premise is carried forward in Figures 16B and C, which graphically depict the degree of coalescence for centerlines of the three sand bodies with the addition of connectedness thresholds of 70 m and 250 m, respectively.

With a threshold of 70 m, the vast majority of centerlines of Exumas and Schooners become interconnected (highlighted gray in Fig. 16B). That is, for these two sand bodies, only a moderate increase in grain production (i.e., sufficient to bridge channels with width < 70 m) causes the sandbars to become fully connected. By contrast, for TOTO, strong coalescence is observed only in the easterly zone, a region where sandbar orientation is particularly chaotic. It takes the imposition of a 250 m connectedness threshold for the majority of TOTO centerlines to become fully linked (Fig. 16C).

The upshot of an increase in the interconnectedness of the sandbar centerlines is that the vectors correspondingly become longer. The different patterns of shift from short-disconnected to long-connected centerlines for the three sand bodies are explored in Figure 17.

Here, exceedance probability (EP) is a measure of the probability (y axis) that a centerline is greater than or equal to a given length value (x axis). When the raw data are considered (i.e., without the imposition of any threshold of connectedness) it can be seen that centerlines of length < 1000 m are very prevalent in the three sand bodies, whereas lines exceeding this length are rare (Fig. 17A). The probability of encountering

←

FIG. 16.—**A)** Example of three different ways of considering centerline connectedness for a flood tidal delta in the Exumas. The imposition of a connectedness threshold serves to increase the degree of linkage, the length, and the number of bifurcations (i.e., complexity) of the centerline composites. The degree of coalesce of sandbar centerlines affected by imposing a connectedness threshold of **B)** 70 m and **C)** 250 m. Not to scale.

lines of a given length are however not consistent between sand bodies. For example, in Exumas there is a 10% likelihood of encountering a centerline of 2000 m length, but in contrast, this probability corresponds to lengths of 4000 m in Schooners and 8000 m for TOTO. The differences in behavior arise by virtue of the different extents for each sand body. With a 70 m connectedness threshold imposed, the change in the distribution of centerline lengths is comparatively minor for Exumas and TOTO, whereas Schooners shows a pronounced shift, with the probability of encountering very long centerlines considerably raised (Fig. 17B, C). The plots confirm the observation made in Figure 16 that a disproportionally large number of lines in the Schooners coalesce when only a 70 m threshold is imposed. That is, the centerlines of Schooners are packed more tightly as compared to the other two sand bodies.

DISCUSSION

Given that grainstones constitute major hydrocarbon reservoirs worldwide, quantitative morphometric characterization of the geometry and size distribution of grainstone geobodies is valuable for exploration and production optimization. Beyond revealing architectural trends that may be of use in reservoir characterization, morphometric analysis of modern geobodies may also provide insight into the processes controlling their distribution and sculpting their geometry. Some results from this study are in accordance with those conducted elsewhere. For example, diversity in shape with body area has similarly been reported in depositional environments ranging from tidal flats to reefs (Rankey 2002; Purkis et al. 2007; Harris and Vlaswinkel 2008). Other trends from the GBB dataset, such as the frequency distributions of sandbars and crests, are poised to provide insight to discussions in the literature that remain the topic of hot debate. For example, it is now well accepted that thin lithologic units typically greatly outnumber the occurrence of thick units in vertical successions of carbonate facies. Similarly, in plan-view facies mosaics of modern carbonate environments, small geobodies are more prevalent than large. The nature of the statistical distributions that link the decline in prevalence with increasing thickness/area are however not understood well. This study provides much needed insight into this question by compiling data from an environment that as of yet has not been interrogated morphometrically, i.e., carbonate sand bodies.

Figure 7 communicates two important pieces of information: (1) it can be seen that the frequency-area distributions of sandbars and bar crests for the three sand bodies considered are not power-law distributed, and (2) an exponential model is shown to capture the trend of the data excellently. Between the three sites, the rate of decay of this model (p) is rather systematic (Fig. 7B, C). Firstly, at each site, crests have a higher p than the sandbars. Secondly, for the two sand bodies which are similarly sized, Schooners and Exumas, the distribution of the model's failure rate is very similar between sandbars and bar crests; Schooners and Exumas sandbars have $p = 1.76$ and 1.52, while p for the crests $= 3.16$ and $3.25 / 10^3$ m^2. Thirdly, TOTO, which is an order larger than the other two sand bodies, returns considerably lower values of p for both its sandbars and bar crests (0.81 and $1.55/10^3$ m^2, respectively). If the geobodies in the dataset were equidimensional in shape (e.g., circular or square)—which they clearly are not (Figure 8)—these values of p would represent the probability of crossing the boundary of a sandbar or bar crest per linear meter of an arbitrary transect lain across the plan-view map (McElroy et al. 2005).

Historically, when an exponential frequency distribution is observed in a vertical succession of facies and/or a plan-view mosaic, it is interpreted as evidence for a random arrangement of thicknesses or areas, widths, or lengths, akin to that which would arise from a Poisson process of lithofacies accumulation (Drummond and Dugan 1999; Wilkinson et al. 1999; Wilkinson and Drummond 2004; Burgess and Wright 2008). The existence of an exponential frequency distribution for this study is unmistakable, and it is appropriate to conclude that the heterogeneity in area of the sandbars and bar crests depicted in Figure 7 is indistinguishable from random at the local scale (i.e., within a sand body). This is not to say, of course, that the distribution of sand bodies atop the GBB is random; their positioning is in fact rather deterministic, parallel to the platform edge and within regions of high tidal energy (Fig. 1).

In order to frame this study with comparable works, it must be kept in mind that there can be a subtle but important difference between the trends of the vertical and spatial lithologic frequency distributions provided by the literature. Thickness defines the vertical extent of stratal elements. By contrast, the extent of a mosaic element in a plan-view facies map can be quantified by either length or width (i.e., 1-D) or area (2-D). Assuming that the mosaic elements are strictly equidimensional, as would be the case in a stationary seascape, the latter is the square of the former. As pointed out by Drummond and Dugan (1999), the implication of the different measures is that a negative exponential trend that links the abundance of *equidimensional* mosaic elements versus their length or width, approximates to a power law if the length or width parameter is squared to area. This extension is inappropriate in this case, given the existence of ample evidence from contemporary carbonate depositional systems of nonstationarity and that geobody shape varies with area and regardless of extent, does not approximate to an equidimensional form (Rankey 2002; Purkis et al. 2007; Harris and Vlaswinkel 2008). With this in mind, the negative exponential distributions reported by (1) this study, (2) the lithofacies extents in ancient carbonate strata (Drummond 1999; Wilkinson et al. 1997, 1998, 1999; Carlson and Grotzinger 2001; Burgess and Wright 2008), and (3) contemporary carbonate facies in plan-view mosaics (Drummond and Dugan 1999; Wilkinson and Drummond 2004) must be considered as genetically different from the power law facies distributions reported from the analysis of high-resolution satellite imagery (Rankey 2002; Harris and Vlaswinkel 2008; Purkis and Kohler 2008; Fullmer et al. 2010; Purkis et al. 2005; Purkis et al. 2007; Purkis et al. 2010). Until this study, it would have been reasonable to perhaps assume the exponential distribution to be an artifact arising from the vagaries of preservation in stratigraphic sequences and inaccuracies in the hand-drawn facies maps considered by Drummond and Dugan (1999) and Wilkinson and Drummond (2004). This now seems unlikely given that the maps created by this study, which, through the use of well-calibrated satellite imagery, can be considered robust, clearly display an exponential and not a power-law frequency distribution for geobody areas.

An important difference does exist between this study and those that have gone before. The geobodies considered are not part of a contiguous mosaic and do not juxtapose one another—the sandbars and their bar crests are separated by "empty" space. Our interrogation of a sparse spatial dataset is atypical, with the majority of comparable studies considering the geometry of contiguous facies mosaics composed of categorical variables (integer facies codes) (Drummond and Dugan 1999; Rankey 2002; Wilkinson and Drummond 2004; Purkis et al. 2005; Purkis et al. 2007; Purkis et al. 2010; Harris and Vlaswinkel 2008; Fullmer et al. 2010; Kaczmarek et al. 2010). The principal difference being that as discussed by Purkis et al. (2007) (p. 506), the scaling of the different facies that compose a contiguous facies mosaic can be controlled, or at least highly augmented, by the frequency and shape distributions of the most common, or architecturally most dominant, facies. Purkis et al. (2007) attributed the power-law scaling observed for $> 7{,}000$ km^2 of shallow-water habitat in the U.S. territorial Pacific to be controlled by the geometries of reefs. The sandbars considered in this study are different in that their shapes and sizes are not related to the sediments of the shelf atop which they are found. Their geometry is instead resultant from, among other factors, the positioning of islands (particularly the case for Exumas), tidal channels, the energy and seawater chemistry regime along the periphery of the GBB, and likely also the geometry of the underlying Pleistocene surface. Under such different controls, it is not surprising therefore that the architecture of the geobodies is dissimilar to reefal

systems. Indeed, some of the frequency distributions plotted by Rankey (2002) (p. 597, his fig. 5) for facies areas of the modern tidal flats of northwest Andros Island, like this study, also seem to depart from clean, pure power laws and follow what appears to be an exponential trend. Though our GBB study is informative, it is not yet possible to ascertain why some seascapes develop power laws, while others, exponentials. However, what is now clear is that both the exponential and power-law frequency distributions can be expected to arise in modern, and thus likely also ancient, carbonate depositional environments. Both distributions are variations on a now common theme of prevalent small geobodies coupled to a predictable decline for the large end of the series. From a modeling perspective, while different, both distributions are mathematically predictable, with the scaling factor m the defining statistic in the case of a power-law trend, and p for the exponential trend. Reassuringly, and as previously recognized for m (Rankey 2002; Purkis et al. 2005; Purkis et al. 2010), the magnitude of p appears to be well behaved and related to the facies under consideration.

A diagnostic signature of a Poisson process in a stratigraphic succession is when the probability of encountering a facies change along-section is independent of the distance to the other horizons of lithologic change in the sample (Wilkinson et al. 1999). Extension of this principle to plan-view mosaics pins the signature of an exponential distribution of lateral facies boundaries to be the existence of a preferred set of geobody areas, but randomly delimited in space. In both the vertical and lateral case, the frequency distribution of the separation of boundaries between stratal elements is exponential, and perceptible ordering of elements in space and/or time, absent. Considered in this way, the exponential distribution is ''memory-less'' and thus exhibits the Markov property (Krumbein and Dacey 1969; Davis 2002). That is, given the present lithology in a stratigraphic sequence, the probability of encountering future lithologies is independent of those previously audited. A random variable with an exponential distribution hence has the Markov property. Though the two observations are rarely convolved, it is of no surprise therefore that while exponential distributions are frequently reported for vertical and lateral carbonate sequences from both the modern and ancient, so are Markov chains (Lehrmann and Rankey 1999; Purkis et al. 2005; Bosence et al. 2009; Riegl and Purkis 2009; Verwer et al. 2009; O'Leary et al. 2009).

SUMMARY

The three sand deposits of GBB that are the focus of this study show a range of depositional facies patterns found in modern sand bodies and their ancient counterparts. TOTO, the broadest expanse of ''high-energy'' sands found in the Bahamas, is characterized by narrow sandbars separated by wide, deep channels and a lack of islands. A variation of this motif in Schooners contains broader and more irregular sandbars with relatively deep and narrow channels and few small islands. And sands associated with tidal channels and the numerous islands of the Exumas occur primarily as flood tidal deltas.

Each sand body is analyzed for size and spatial patterns. In order to examine the variation within the sand body, different water-depth intervals are selected and contoured to define polygons that represent individual sandbars and bar crests. Centerlines visually interpreted along the crests of the sandbars using the bathymetric DEM provide methods of capturing information that are alternative to that of the contour-based sandbar polygons. Observations and quantitative relations developed in this study are as follows:

- The breadth of the tidal channels that separate sandbars is more consistent between the three sand bodies than the width of the sandbars themselves, as shown by FFT of sand body profiles. The average separation between sandbars falls within a narrow threshold of only a few hundred meters, regardless of the site considered.
- While the spatial distribution of sandbars between the three sand bodies is variable, the relative proportion of area occupied by bar crests (assumed to be well-sorted grainstones) with respect to the area of sandbars (less well-sorted grainstones) is very consistent. A consistent proportional representation of the area covered by the two features is surprising, especially given the differences in morphology between the three sand bodies.
- The frequency-area relationship of sandbars and bar crests is exponential. Such a distribution would arise from a population of bodies with a preferred set of areas but randomly delimited in space.
- Small sandbars tend to be rounded, as quantified by the form factor, whereas large (> 1 km^2) are exclusively elongate.
- Particularly strong trends were observed when the distance to platform edge was compared to the mean and variance in depth of sandbars. The tops of sandbars in close proximity to the platform edge tend to be, on average, deeper than those found more distally, whereas the greatest variances in depth are returned by sandbars in close proximity to the edge.
- More rounded sandbars are found within close proximity to one another, while those separated by great distance have a tendency to be elongate. The size of a sandbar has no bearing on the separating distance to the nearest neighbor; however, more separated sandbars have a distinctly lower variance in water depth.
- There is a clear trend such that the sandbars with the roughest surfaces (i.e., most thickness variation) tend to be of greatest area.
- The ratios of surface to planar areas of the sandbars are well behaved with respect to the distance setback from the platform edge.
- TOTO and Schooners, the two sand bodies without islands, have very similar sandbar centerline density (32% and 35%, respectively), whereas the island-rich Exumas has a relatively lower centerline density (21%).
- Sandbar centerlines at Schooners and TOTO have almost identical fractal complexity; Exumas centerlines are considerably less complex. All sites show the same pattern in that simple centerlines are by far the most prevalent while each site displays a small number of highly complex and convoluted sandbar lines (< 50, or $\sim 25\%$ of total). That is, the tendency for the formation of sinuous and intricate centerlines is similar between the sand bodies, suggesting similar mechanisms at play in each setting.
- We can quantify the degree of connectivity between the individual sandbar centerline segments for each site, linking changes in potential rates of grain production to gaps between centerlines. For instance, the vast majority of centerlines of Exumas and Schooners become interconnected with a connectedness threshold of 70 m. That is, for these two sand bodies, only a moderate increase in grain production (i.e., sufficient to bridge channels with width < 70 m that now separate individual sandbars) causes the sandbars to become fully connected. By contrast, for TOTO it takes the imposition of a 250 m connectedness threshold for the majority of TOTO centerlines to become fully linked.

The study is an attempt to highlight how morphometric interrogation can yield quantitative information on complex depositional environments, in this case sand bodies and sandbars. The approach allows a description that would ordinarily have been reported in many words to be distilled to a small number of numeric indices. As previously observed in reefal systems, several geometric aspects of high-energy sand deposits also appear to be rather generic. We think that such results broaden our perspective of the types of information that can be derived from studies of the modern.

ACKNOWLEDGMENTS

We thank Chevron Energy Technology Company for support of this research and for permission to publish. We acknowledge the following for

data that was critical to our work: Global Land Facility Center (GLFC) for SRTM DEMs; USGS Earth Explorer for Landsat TM imagery; Lewis Offshore Ltd. (www.explorercharts.com) for their navigation charts; and Gene Rankey for providing soundings in southeastern Schooners. We are grateful for the assistance that Kevin Kohler provided in the programming of algorithms for the morphometric interrogation of geobodies. We are grateful for the highly constructive and useful reviews to this paper returned by Carl Drummond, Sal Mazzullo, and JSR Associate Editor Robert Goldstein. We are also indebted to JSR Associate Editor Bruce Wilkinson for stimulating discussions on the nature of geobody area-frequency relations.

REFERENCES

Ball, M.M., 1967, Carbonate sand bodies of Florida and the Bahamas: Journal of Sedimentary Petrology, v. 37, p. 556–591.

Bosence, D., Procter, E., Aurell, M., Kahla, A.B., Boudagher-Fadel, M., Casaglia, F., Cirilli, S., Mehdie, M., Nieto, L., Rey, J., Scherreiks, R., Soussi, M., and Waltham, D., 2009, A dominant tectonic signal in high-frequency, peritidal carbonate cycles? A regional analysis of Liassic platforms from western Tethys: Journal of Sedimentary Research, v. 79, p. 389–415.

Burgess, P.M., and Wright, V.P., 2008, The nature of shallow-water carbonate lithofacies thickness distributions: Geology, v. 36, p. 235–238.

Carlson, J., and Grotzinger, J.P., 2001, Submarine fan environment inferred from turbidite thickness distributions: Sedimentology, v. 48, p. 1331–1351.

Davis, J.C., 2002, Statistics and Data Analysis in Geology, Third Edition: New York, John Wiley and Sons, 637 p.

Dravis, J.J., 1977. Holocene sedimentary depositional environments on Eleuthera Bank, Bahamas [Unpublished M.S. Thesis]: University of Miami, Miami, Florida, 386 p.

Drummond, C.N., 1999, Bed thickness structure of multi-sourced ramp turbidites: Devonian Braillier Formation, central Appalachian Basin: Journal of Sedimentary Research, v. 69, p. 115–121.

Drummond, C.N., and Dugan, P.J., 1999, Self-organizing models of shallow-water carbonate accumulation: Journal of Sedimentary Research, v. 69, p. 939–946.

Enos, P., 1974. Surface sediment facies of the Florida–Bahamas Plateau: Geological Society of America, Map Series MC-5, Fourth Edition.

Fullmer, S., Kaczmarek, S.E., and Steffen, K., 2010, Modern carbonate facies: moving from description to quantitative prediction: Seismic Imaging of Depositional and Geomorphic Systems: Gulf Coast Section, SEPM Foundation, 30th Annual Bob F. Perkins Research Conference, December 5–8 2010, Houston, Texas.

Halley, R.B., Harris, P.M., and Hine, A.C., 1983, Bank margin environments, *in* Scholle, P.A., Bebout, D.G., and Moore, C.H., eds., Carbonate Depositional Environments: American Association of Petroleum Geologists, Memoir 33, p. 463–506.

Harris, P.M., 1979, Facies anatomy and diagenesis of a Bahamian ooid shoal: University of Miami, Miami, Florida, Comparative Sedimentology Laboratory, Sedimenta 7, 163 p.

Harris, P.M., 2010, Delineating and quantifying depositional facies patterns in carbonate reservoirs: insight from modern analogs: American Association of Petroleum Geologists, Bulletin, v. 94, p. 61–86.

Harris, P.M., and Kowalik, W.S., eds. 1994, Satellite Images of Carbonate Depositional Settings: Examples of Reservoir- and Exploration-Scale Geologic Facies Variation: American Association of Petroleum Geologists, Methods in Exploration Series 11, 147 p.

Harris, P.M., and Vlaswinkel, B.M., 2008, Modern isolated carbonate platforms: templates for quantifying facies attributes of hydrocarbon reservoirs, *in* Lukasik, J., and Simo, T., eds., Controls on Carbonate Platform and Reef Development: SEPM, Special Publication 89, p. 323–341.

Harris, P.M., and Ellis, J.M., 2009, Satellite imagery, visualization and geologic interpretation of the Exumas, Great Bahamas Bank – an analog for carbonate sand reservoirs: SEPM (Society for Sedimentary Geology), Short Course Notes 53, p. 1–49 and 2 DVDs.

Harris, P.M., Ellis, J.M., and Purkis, S.J., 2010, Delineating and quantifying depositional facies patterns of modern carbonate sand deposits on Great Bahama Bank: SEPM, Short Course Notes 54, p. 1–51, appendix p. 1–31, and 2 DVDs.

Hine, A.C., 1977, Lily Bank, Bahamas: history of an active oolite sand shoal: Journal of Sedimentary Petrology, v. 47, p. 1554–1581.

Kaczmarek, S.E., Hicks, M.K., Fullmer, S.M., Steffen, K.L., and Bachtel, S.L., 2010, Mapping facies distributions on modern carbonate platforms through integration of multispectral Landsat data, statistics-based unsupervised classifications, and surface sediment data: American Association of Petroleum Geologists, Bulletin, v. 94, p. 1581–1606.

Krumbein, W.C., and Dacey, M.F., 1969, Markov chains and embedded Markov chains in geology: International Association for Mathematical Geology, Journal, v. 1, p. 79–96.

Lehrmann, D.J., and Rankey, E.C., 1999, Do meter-scale cycles exist? A statistical evaluation from vertical (1-D) and lateral (2-D) patterns in shallow-marine carbonates–siliciclastics of the "fall in" strata of the Capitan Reef, Seven Rivers Formation, Slaughter Canyon, New Mexico, *in* Saller, A.H., Harris, P.M., Kirkland, B.L., and Mazzullo, S.J., eds., Geologic Framework of the Capitan Reef: SEPM, Special Publication 65, p. 51–62.

McElroy, B.J., Wilkinson, B.H., and Rothman, E.D., 2005, Tectonic and topographic framework of political division: Mathematical Geology, v. 37, p. 197–206.

McNeill, D.F., Eberli, G.P., Harris, P.M., and Cruz, F.E.G., 2004. Field Guide to Carbonate Sediments along the Exuma Bank Margin, and a Virtual Fieldtrip to the Exuma Island Chain, Bahamas: University of Miami, Miami, Florida, Comparative Sedimentology Laboratory, Sedimenta CD, series no. 2.

Newell, N.D., Purdy, E.G., and Imbrie, J., 1960, Bahamian oolitic sand: Journal of Geology, v. 68, p. 481–496.

O'Leary, M.A., Perry, C.T., Beavington-Penney, S.J., and Turner, J.R., 2009, The significant role of sediment bio-retexturing within a contemporary carbonate platform system: implications for carbonate microfacies development: Sedimentary Geology, v. 219, p. 169–179.

Palmer, M.S., 1979, Holocene facies geometry of the leeward bank margin, Tongue of the Ocean, Bahamas [Unpublished M.S. Thesis]: University of Miami, Miami, Florida, 199 p.

Purdy, E.G., 1961, Bahamian oolite shoals, *in* Peterson, J.A., and Osmond, J.C., eds., Geometry of Sandstones Bodies: American Association of Petroleum Geologists, Symposia, v. Special Publication 22, p. 53–62.

Purdy, E.G., 1963, Recent calcium carbonate facies of the Great Bahama Bank, 2. Sedimentary facies: Journal of Geology, v. 71, p. 472–497.

Purkis, S.J., and Kohler, K.E., 2008, The role of topography in promoting fractal patchiness in a carbonate shelf landscape: Coral Reefs, v. 27, p. 977–989.

Purkis, S.J., Reigl, B.M., and Andréfouët, S., 2005, Remote sensing of geomorphology and facies patterns on a modern carbonate ramp (Arabian Gulf, Dubai, U.A.E.): Journal of Sedimentary Research, v. 75, p. 861–876.

Purkis, S.J., Kohler, K.E., Riegl, B.M., and Rohmann, S.O., 2007, The statistics of natural shapes in modern coral reef landscapes: Journal of Geology, v. 115, p. 493–508.

Purkis, S.J., Rowlands, G.P., Riegl, B.M., and Renaud, P.G., 2010, The paradox of tropical karst morphology in the coral reefs of the arid Middle East: Geology, v. 38, p. 227–230.

Rankey, E.C., 2002, Spatial patterns of sediment accumulation on a Holocene carbonate flat, northwest Andros Island, Bahamas: Journal of Sedimentary Research, v. 72, p. 591–601.

Rankey, E.C., Riegl, B.M., and Steffen, K., 2006, Form, function, and feedbacks in a tidally dominated ooid shoal, Bahamas: Sedimentology, v. 53, p. 1191–1210.

Rankey, E.C., Reeder, S.L., Ritter, S., and Harris, P.M., 2008, Morphology and dynamics of carbonate tidal sand ridges: Schooner Cays, Bahamas: American Association of Petroleum Geologists, International Conference, Abstracts Volume, p. 32. (posted in 2008 on AAPG Search and Discovery as Article #50134).

Reeder, S.L., and Rankey, E.C., 2008, Interactions between tidal flows and ooid shoals, northern Bahamas: Journal of Sedimentary Research, v. 78, p. 175–186.

Reeder, S.L., and Rankey, E.C., 2009, Controls on morphology and sedimentology of carbonate tidal deltas, Abacos, Bahamas: Marine Geology, v. 267, p. 141–155.

Reijmer, J.J.G., Swart, P.K., Bauch, T., Otto, R., Reuning, L., Roth, S., and Zechel, S., 2009, A re-evaluation of facies on Great Bahama Bank I: new facies maps of western Great Bahama Bank, *in* Swart, P.K., Eberli, G.P., and McKenzie, J.A., eds., Perspectives in Carbonate Geology: A Tribute to the Career of Robert Nathan Ginsburg: International Association of Sedimentologists, Special Publication 41, p. 29–46.

Riegl, B., and Purkis, S.J., 2009, Markov models for linking facies in space and time (Arabian Gulf, Miocene Paratethys), *in* Swart, P.K., Eberli, G.P., and McKenzie, J.A., eds., Perspectives in Sedimentary Geology: A Tribute to the Career of Robert Nathan Ginsburg: International Association of Sedimentologists, Special Publication 41, p. 337–360.

Russ, J.C., 1999, The Image Processing Handbook, Third Edition: Boca Raton, Florida, CRC Press, 717 p.

Traverse, A., and Ginsburg, R.N., 1966, Palynology of the surface sediments of Great Bahama Bank, as related to water movement and sedimentation: Marine Geology, v. 4, p. 417–459.

Verwer, K., Della Porta, G., Merino-Tomé, O., and Kenter, J.A.M., 2009, Controls and predictability of carbonate facies architecture in a Lower Jurassic three-dimensional barrier-shoal complex (Djebel Bou Dahar, High Atlas, Morocco): Sedimentology, v. 56, p. 1801–1831.

Wilkinson, B.H., and Drummond, C.N., 2004, Facies mosaics across the Persian Gulf and around Antigua—stochastic and deterministic products of shallow-water sediment accumulation: Journal of Sedimentary Research, v. 74, p. 513–526.

Wilkinson, B.H., Drummond, C.N., Diedrich, N.W., and Rothman, E.D., 1997, Biological mediation of stochastic peritidal carbonate accumulation: Geology, v. 25, p. 847–850.

Wilkinson, B.H., Diedrich, N.W., Drummond, C.N., and Rothman, E.D., 1998, Michigan hockey, meteoric precipitation, and rhythmicity of accumulation on peritidal carbonate platforms: Geological Society of America, Bulletin, v. 110, p. 1075–1093.

Wilkinson, B.H., Drummond, C.N., Diedrich, N.W., and Rothman, E.D., 1999, Poisson processes of carbonate accumulation on Paleozoic and Holocene platforms: Journal of Sedimentary Research, v. 69, p. 338–350.

Received 8 June 2010; accepted 27 October 2010.